MIT Joint Program on the Science and Policy of Global Change

Probabilistic Forecast for 21st Century Climate Based on Uncertainties in Emissions (without Policy) and Climate Parameters

A.P. Sokolov, P.H. Stone, C.E. Forest, R. Prinn, M.C. Sarofim, M. Webster, S. Paltsev, C.A. Schlosser, D. Kicklighter, S. Dutkiewicz, J. Reilly, C. Wang, B. Felzer, J. Melillo, and H.D. Jacoby

Report No. 169
January 2009

The MIT Joint Program on the Science and Policy of Global Change is an organization for research, independent policy analysis, and public education in global environmental change. It seeks to provide leadership in understanding scientific, economic, and ecological aspects of this difficult issue, and combining them into policy assessments that serve the needs of ongoing national and international discussions. To this end, the Program brings together an interdisciplinary group from two established research centers at MIT: the Center for Global Change Science (CGCS) and the Center for Energy and Environmental Policy Research (CEEPR). These two centers bridge many key areas of the needed intellectual work, and additional essential areas are covered by other MIT departments, by collaboration with the Ecosystems Center of the Marine Biology Laboratory (MBL) at Woods Hole, and by short- and long-term visitors to the Program. The Program involves sponsorship and active participation by industry, government, and non-profit organizations.

To inform processes of policy development and implementation, climate change research needs to focus on improving the prediction of those variables that are most relevant to economic, social, and environmental effects. In turn, the greenhouse gas and atmospheric aerosol assumptions underlying climate analysis need to be related to the economic, technological, and political forces that drive emissions, and to the results of international agreements and mitigation. Further, assessments of possible societal and ecosystem impacts, and analysis of mitigation strategies, need to be based on realistic evaluation of the uncertainties of climate science.

This report is one of a series intended to communicate research results and improve public understanding of climate issues, thereby contributing to informed debate about the climate issue, the uncertainties, and the economic and social implications of policy alternatives. Titles in the Report Series to date are listed on the inside back cover.

Henry D. Jacoby and Ronald G. Prinn,
Program Co-Directors

For more information, please contact the Joint Program Office

Postal Address: Joint Program on the Science and Policy of Global Change
400 Main Street
MIT E19-411
Cambridge MA 02139-4307 (USA)

Location: 400 Main Street, Cambridge
Building E19, Room 411
Massachusetts Institute of Technology

Access: Phone: +1(617) 253-7492
Fax: +1(617) 253-9845
E-mail: globalchange@mit.edu
Web site: http://globalchange.mit.edu/ /

Printed on recycled paper

Probabilistic Forecast for 21st Century Climate Based on Uncertainties in Emissions (without Policy) and Climate Parameters

A.P. Sokolov[*], P.H. Stone[*], C.E. Forest[*], R. Prinn[*], M.C. Sarofim[*], M. Webster[*], S. Paltsev[*], C.A. Schlosser[*], D. Kicklighter[†], S. Dutkiewicz[*], J. Reilly[*], C. Wang[*], B. Felzer[‡], J. Melillo[†], and H.D. Jacoby[*]

Abstract

The MIT Integrated Global System Model is used to make probabilistic projections of climate change from 1861 to 2100. Since the model's first projections were published in 2003 substantial improvements have been made to the model and improved estimates of the probability distributions of uncertain input parameters have become available. The new projections are considerably warmer than the 2003 projections, e.g., the median surface warming in 2091 to 2100 is 5.1°C compared to 2.4°C in the earlier study. Many changes contribute to the stronger warming; among the more important ones are taking into account the cooling in the second half of the 20th century due to volcanic eruptions for input parameter estimation and a more sophisticated method for projecting GDP growth which eliminated many low emission scenarios. However, if recently published data, suggesting stronger 20th century ocean warming, are used to determine the input climate parameters, the median projected warning at the end of the 21st century is only 4.1°C. Nevertheless all our simulations have a very small probability of warming less than 2.4°C, the lower bound of the IPCC AR4 projected likely range for the A1FI scenario, which has forcing very similar to our median projection. The probability distribution for the surface warming produced by our analysis is more symmetric than the distribution assumed by the IPCC due to a different feedback between the climate and the carbon cycle, resulting from a different treatment of the carbon-nitrogen interaction in the terrestrial ecosystem.

Contents

[*] MIT Joint Program on the Science and Policy of Global Change (E-mail: Sokolov@mit.edu)
[†] The Ecosystems Center, Marine Biological Laboratory
[‡] Department of Earth and Environmental Sciences, Lehigh University

1. INTRODUCTION

Projections of anthropogenic global warming have from the start been confounded by the many economic and scientific uncertainties that affect forecasts of anthropogenic emissions and the response of the climate system to these emissions (e.g., Houghton *et al*. 2001 and Solomon *et al*. 2007). Up until 2001, the uncertainties in the projected climate changes were generally dealt with by giving ranges of projected changes, but without any likelihoods being associated with these ranges. Such projections leave it to the non-expert reader to assign probabilities to the possible outcomes; Moss and Schneider (2000) advocated that projections should be given in probabilistic terms to provide more complete information.

Subsequently, considerable effort has been devoted to quantifying the scientific uncertainties associated with climate model projections for a given forcing scenario. Most notably the latest IPCC report (Meehl *et al*. 2007a) attempted to do this for the six SRES scenarios (Nakicenovic *et al*. 2000) using a variety of coupled atmosphere-ocean general circulation models (AOGCMs) and models of intermediate complexity. These projections and different sources of uncertainty have been reviewed by Knutti *et al*. (2008).

While formal uncertainty analysis of emissions projections was investigated a couple of decades ago (e.g. Nordhaus and Yohe 1983; Edmonds and Reilly 1985; Reilly *et al*. 1987) it was largely ignored by the scientific community. The IPCC SRES process eschewed formal uncertainty analysis of emissions in favor of scenario analysis (Nakicenovic *et al*. 2000). Despite clear statements to the contrary (Nakicenovic *et al*. 2000) there have been attempts in the literature to interpret the SRES scenarios in a probabilistic or quasi-probabilistic sense to investigate the joint effects of uncertainty in emissions and climate outcomes (e.g. Wigley and Raper 2001). In the latest IPCC report uncertainty ranges for possible climate changes are given separately for different SRES scenarios and reflect only uncertainty in climate system response (Meehl *et al*. 2007a).

The most comprehensive formal treatment of both emissions and scientific uncertainties to date is that of Webster *et al*. (2003). In that work, uncertainty in emissions projections was driven by uncertainty in future economic growth and technological change (Webster *et al*. 2002) as well as uncertainty in current levels of emissions (Olivier and Berdowski 2001). The climate system uncertainties were quantified from an analysis of observed 20th century temperature changes (Forest *et al*. 2002).

In this paper, we update the Webster *et al*. (2003) probabilistic projections of climate change from the present to 2100. The Webster *et al*. (2003) used the MIT Integrated Global System Model (IGSM, Prinn *et al*. 1999), which couples an economic component (the MIT Emissions Prediction and Policy Analysis model, EPPA (Babiker *et al*. 2001) to a climate model of

intermediate complexity (Sokolov and Stone 1998; Wang *et al*. 1998).

The IGSM was designed to be flexible and numerically efficient and so is well-suited for use in making probabilistic projections. For example, its climate sensitivity can be varied by changing its cloud feedback and the rate of penetration of heat into the deep ocean can be varied by changing an appropriate mixing coefficient (Sokolov *et al*. 2005). This flexibility allows us to avoid, to a considerable extent, the structural rigidity that limits the ability of individual coupled AOGCMs to assess uncertainty in projections of global change. Also, the use of parameters' distributions as constrained by 20th century temperature changes allows us to cover full uncertainty ranges for the climate system properties controlled by the model parameters. The economic and emissions component of the IGSM is driven by growth in the general economy and includes representation of final consumption and trade in all goods services, including a relatively detailed treatment of factors driving emissions from energy, agriculture, waste and industrial sources as they depend on resource availabilities and technological alternatives (Paltsev *et al*. 2005). The IGSM was used as part of the recent US CCSP scenarios exercise to generate a set of new global scenarios of emissions with and without policy intervention (CCSP 2007) and so this work extends the scenario approach applied there to a probabilistic analysis.

Since Webster *et al*. (2003) was published, the IGSM has been upgraded as described by Sokolov *et al*. (2005). These upgrades include an increase in resolution of the atmospheric model, replacement of a zonally-averaged mixed layer ocean model by a latitude-longitude resolving one, implementation of more sophisticated land system model, and a more detailed representation of the national and regional economies of the world. In addition to the improvements made to the IGSM itself, the results presented here are based on a new analysis of factors contributing to uncertainty in emissions (Webster *et al*. 2008). Simulations of 20th century climate used to derive distributions of earth system properties (Forest *et al*. 2008) were carried out with a more complete set of natural and anthropogenic forcings than simulations used by Forest *et al*. (2002).

These changes led to relatively moderate changes in the distributions of both the projected emissions and the climate system's response to a given forcing. However, due to nonlinear interactions between these factors, the net effect has been to shift the distributions of warming and sea level rise substantially upward when compared to Webster *et al*. (2003). As discussed in detail in later sections, the overall shift in the distribution, which doubles the previous median estimate of warming, has no single major contributing factor but rather results from the combination of several changes.

One critical factor to consider is the source of the input distributions and the sensitivity of any results to them. In particular, the distributions presented by Forest *et al*. (2008) were obtained using estimates of changes in deep ocean heat content for the 0-3000 m layer provided by Levitus *et al*. (2005). A recent update of the Levitus *et al*. (2005) analysis (given on the NOAA website) corrects for errors in the XBT data pointed out by Gouretski and Koltermann (2007), but nevertheless obtains virtually the same result as the original analysis. However Gouretski and Koltermann (2007) and Domingues *et al*. (2008), who also attempt to take into

account these errors, come up with different estimates of changes in the ocean heat content for the 0-3000 m layer. Sokolov *et al*. 2008b have shown that projections of future climate change are sensitive to the distributions of climate model parameters derived using these alternative estimates of the changes in deep-ocean heat content. For consistency with our earlier study (Webster *et al*. 2003) we carried out our simulations using the climate parameter distributions based on the analysis of Levitus *et al*. (2005). However, given the significant influence of the estimate of the ocean heat uptake on the projections, we also discuss the sensitivity of our results to other estimates of the changes in the heat content of the deep ocean.

The outline of the paper is as follows. In section 2 the updated IGSM is described. Then in section 3 we present our methodology, enumerating the uncertainties taken into account, how they are characterized, and how the probabilistic projections are made. In section 4 we give our 21st century projections for a variety of indicators of changes in the earth system including greenhouse gas (GHG) concentrations, surface air temperature (SAT) changes, and sea-level rise (SLR) and we compare our results with those of Webster *et al*. (2003) and the IPCC's AR4. Finally we give our conclusions in section 5.

2. MODEL COMPONENTS

The MIT Integrated Global System Model includes sub-models of the relevant parts of the natural earth system and a model of the human activity. A description of the IGSM Version 1, along with sensitivity tests of key aspects of its behavior, was reported in Prinn *et al.* (1999). Version 2 of the IGSM (IGSM2, Sokolov *et al*. 2005) includes the following components (**Figure 1**):

- A model of human activities and emissions (the Emissions Prediction and Policy Analysis Model),
- An atmospheric dynamics, physics and chemistry model, which includes a sub-model of urban chemistry,
- A mixed layer/ anomaly diffusing ocean model (ADOM) with carbon cycle and sea ice sub-models,
- A land system model that combines the Terrestrial Ecosystem Model (TEM), a Natural Emissions Model (NEM), and the Community Land Model (CLM), that together describe the global, terrestrial water and energy budgets and terrestrial ecosystem processes.

The Earth climate system component of the IGSM is a fully coupled model which allows simulation of critical feedbacks between components. The time steps used in the various sub-models range from 10 minutes for atmospheric dynamics to 1 month for TEM, reflecting differences in the characteristic timescales of the various processes simulated by the IGSM.

The IGSM is distinguished from other similar models by its inclusion of significant chemical and biological detail. Our models of the terrestrial carbon, methane and nitrous oxide cycles are coupled to climate, terrestrial hydrology and land ecosystems models, which provide the needed explicit predictions of temperature, rainfall, and soil organic carbon concentrations. The prediction of global anthropogenic emissions of CO_2, CO, NO_x, black carbon, SO_x and other key

species is based on a regionally disaggregated model of global economic growth. This procedure allows for treatment over time of a shifting geographical distribution of emissions, changing mixes of these emissions, and recognition of the fact that the emissions of chemicals important in air pollution and climate are highly correlated due to shared generating processes like combustion.

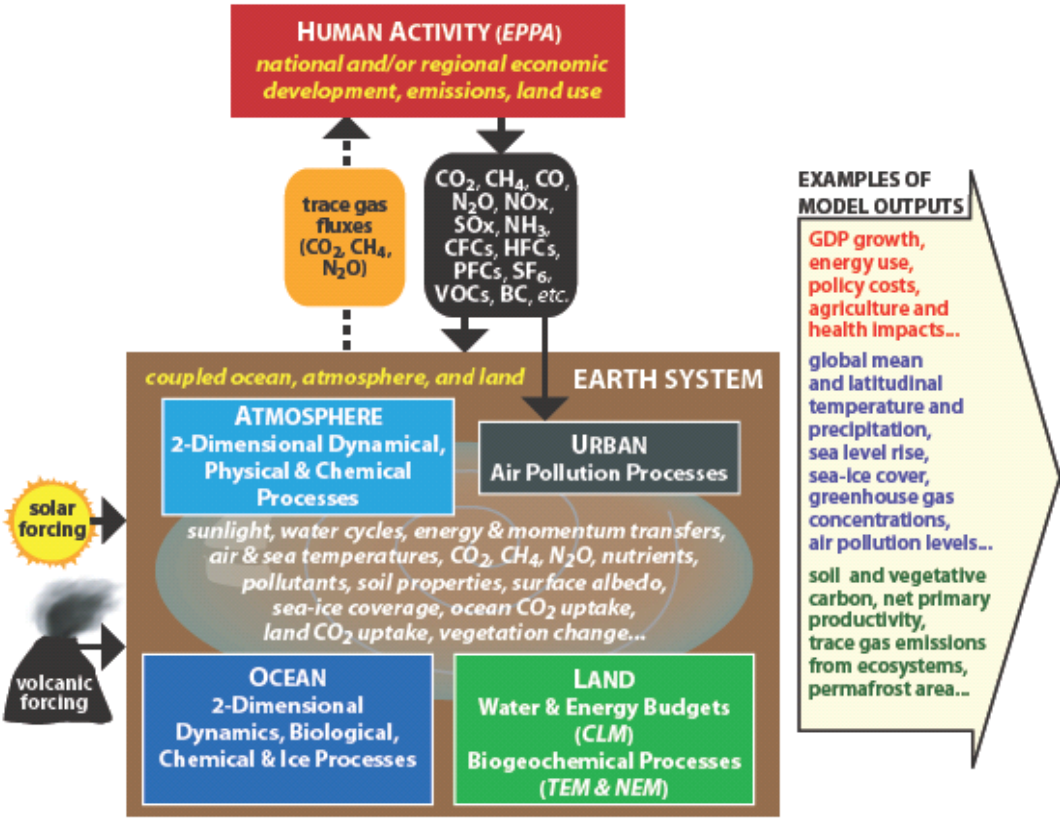

Figure 1. The MIT IGSM version 2.2

The major model components of the IGSM2 and recent developments in their capabilities and linkages are summarized below.

2.1 Human activity and emissions

The Emissions Prediction and Policy Analysis (EPPA) Model is a general equilibrium model of the world economy developed by the MIT Joint Program on the Science and Policy of Global Change (Paltsev *et al*. 2005). For economic data, it relies on the GTAP dataset (Dimaranan and McDougall, 2002), which accommodates a consistent representation of regional macroeconomic consumption, production and bilateral trade flows. The energy data in physical units are based on energy balances from the International Energy Agency. EPPA model also uses additional data for past greenhouse gas emissions (carbon dioxide, CO_2; methane, CH_4; nitrous oxide, N_2O; hydrofluorocarbons, HFCs; perfluorocarbons, PFCs; and sulphur hexafluoride, SF_6) and past air pollutant emissions (sulphur dioxide, SO_2; nitrogen oxides, NO_x; black carbon, BC; organic

carbon, OC; ammonia, NH_3; carbon monoxide, CO; and non-methane volatile organic compounds, VOC) based on United States Environmental Protection Agency inventory data supplemented by our own estimates.

Much of the model's sectoral detail is focused on energy production to represent technological alternatives in electric generation and transportation. From 2000 to 2100 the model is solved recursively at 5-year intervals. The EPPA model production and consumption sectors are represented by nested Constant Elasticity of Substitution (CES) production functions (or the Cobb-Douglas and Leontief special cases of the CES). The model is written in the GAMS software system and solved using MPSGE modeling language (Rutherford 1995). The EPPA model has been used in a wide variety of policy applications (e.g., Jacoby *et al*. 1997; Reilly *et al*. 1999; Babiker *et al*. 2003; Reilly and Paltsev 2006; US CCSP 2007; Paltsev *et al*. 2008).

Because climate and energy policy are our main focus, the model further disaggregates the data for transportation and existing energy supply technologies and as well includes a number of alternative sources that are not in widespread use now, but could take market share in the future under changed energy prices or climate policy conditions. Bottom-up engineering details are incorporated in EPPA model in the representation of these alternative energy supply technologies. The competitiveness of different technologies depends on the endogenously determined prices for all inputs, and those prices depend in turn on depletion of resources, economic policy, and other forces driving economic growth such as savings, investment, energy-efficiency improvements, and productivity of labor. Additional information on the model's structure can be found in Paltsev *et al*. (2005).

2.2 Atmospheric Dynamics and Physics

The MIT two-dimensional (2D) atmospheric dynamics and physics model (Sokolov and Stone 1998) is a zonally averaged statistical-dynamical model that explicitly solves the primitive equations for the zonal mean state of the atmosphere and includes parameterizations of heat, moisture, and momentum transports by large scale eddies based on baroclinic wave theory (Stone and Yao 1987 and 1990). The model's numerics and parameterizations of physical processes, including clouds, convection, precipitation, radiation, boundary layer processes, and surface fluxes, are built upon those of the Goddard Institute for Space Studies (GISS) GCM (Hansen *et al*. 1983). The radiation code includes all significant greenhouse gases (H_2O, CO_2, CH_4, N_2O, CFCs and O_3) and eleven types of aerosols. The model's horizontal and vertical resolutions are variable, but the standard version of IGSM2 has 4° resolution in latitude and eleven levels in the vertical.

The MIT 2D atmospheric model allows up to four different types of underlying surface in each grid cell (ice free ocean, sea-ice, land, and land-ice). The surface characteristics (e.g., temperature, soil moisture, albedo) as well as turbulent and radiative fluxes are calculated separately for surface type. The atmosphere above is assumed to be well mixed zonally in each latitudinal band. The area-weighted fluxes from the different surface types are used to calculate the change of temperature, humidity, and wind speed in the atmosphere. Convection and large-

scale condensation are simulated under the assumptions that a zonal band may be partially unstable or partially saturated, respectively. The moist convection parameterization, which was originally designed for the GISS Model I (Hansen *et al*. 1983), requires knowledge of sub-grid scale temperature variance. Zonal temperature variance associated with transient eddies is calculated using a parameterization proposed by Branscome (see Yao and Stone 1987). The variance associated with stationary eddies was represented in the IGSM1 by adding a fixed variance of 2 K at all latitudes. In the IGSM2 we introduce a latitudinal dependence of the latter variance that follows more closely the climatological pattern (see Figure. 7.8b of Peixoto and Oort 1992). In addition, the threshold values of relative humidity for the formation of large-scale cloud and precipitation have been modified such that a constant value for all latitudes (as used in the IGSM1) is replaced with latitudinally varying values. This modification is made to account for the dependence of the zonal variability of relative humidity on latitude. Zonal precipitations simulated by atmospheric model are partitioned into land and ocean components using present day climatology. These changes led to an improvement in the zonal pattern of the annual cycle of land precipitation and evapotranspiraton (Schlosser at al. 2007).

The atmospheric model's climate sensitivity can be changed by varying the cloud feedback. The method for changing this feedback in the model has been changed from the method used previously. In the IGSM1 the cloud cover at all levels was changed by a fixed fraction, which depended on the global mean surface temperature (Sokolov and Stone 1998). In the IGSM2 high cloud covers and low cloud covers are changed in opposite directions by a constant factor, which is again dependent on the global mean surface temperature. The new method, described by Sokolov (2006), shows better agreement with changes simulated by AOGCMs.

2.3 Atmospheric Chemistry

To calculate atmospheric composition, the model of atmospheric chemistry includes an analysis of the climate-relevant reactive gases and aerosols at urban scales, coupled to a model of the processing of exported pollutants from urban areas (plus the emissions from non-urban areas) at the regional to global scale. For calculation of the atmospheric composition in non-urban areas, the above atmospheric dynamics and physics model is linked to a detailed 2D zonal mean model of atmospheric chemistry. The atmospheric chemical reactions are thus simulated in two separate modules, one for the 2D model grids and one for the sub-grid-scale urban chemistry.

2.3.1 Urban Air Chemistry

The analysis of the atmospheric chemistry of key substances as they are emitted into polluted urban areas is an important addition to the integrated system since the version described in Prinn *et al*. (1999). Urban air pollution is explicitly treated in the IGSM for several reasons. It has a significant impact on global methane, ozone and aerosol chemistry, and thus on climate. However, the nonlinearities in the chemistry cause urban emissions to undergo different net transformations than rural emissions. Accuracy in describing these transformations is necessary because the atmospheric lifecycles of exported air pollutants such as CO, O_3, NO_x and VOCs, and the climatically important species CH_4 and sulfate aerosols, are linked through the fast

photochemistry of the hydroxyl free radical (OH) as we will emphasize in the results discussed later in section 5. Urban air-shed conditions need to be resolved at varying levels of pollution. The urban air chemistry model must also provide detailed information about particulates and their precursors important to air chemistry and human health, and about the effects of local topography and structure of urban development on the level of containment and thus the intensity of air pollution events. This is an important consideration because air pollutant levels are dependent on projected emissions per unit area, not just total urban emissions.

The urban atmospheric chemistry model has been introduced as an additional component to the original global model (Prinn *et al*. 1999) in IGSM1 (Calbo *et al*. 1998; Mayer *et al*. 2000; Prinn *et al*. 2007). It was derived by fitting multiple runs of the detailed 3D California Institute of Technology (CIT) Urban Airshed Model, adopting the probabilistic collocation method to express outputs from the CIT model in terms of model inputs using polynomial chaos expansions (Tatang *et al.* 1997). This procedure results in a reduced format model to represent about 200 gaseous and aqueous pollutants and associated reactions over urban areas that is computationally efficient enough to be embedded in the global model. The urban module is formulated to take meteorological parameters including wind speed, temperature, cloud cover, and precipitation as well as urban emissions as inputs. Calculated with a daily time step, it exports fluxes along with concentrations (peak and mean) of selected pollutants to the global model.

2.3.2 Global Atmospheric Chemistry

The 2D zonal mean model that is used to calculate atmospheric composition is a finite difference model in latitude-pressure coordinates, and the continuity equations for trace constituents are solved in mass conservative or flux form (Wang *et al*. 1998). The model includes 33 chemical species. The continuity equations for $CFCl_3$, CF_2Cl_2, N_2O, O_3, CO, CO_2, NO, NO_2, N_2O_5, HNO_3, CH_4, CH_2O, SO_2, H_2SO_4, HFC, PFC, SF_6, black carbon aerosol, and organic carbon aerosol include convergences due to transport, parameterized north-south eddy transport, convective transports, local true production or loss due to surface emission or deposition, and atmospheric chemical reactions. In contrast to these gases and aerosols, the very reactive atoms (e.g., O), free radicals (e.g., OH), or molecules (e.g., H_2O_2) are assumed to be unaffected by transport because of their very short lifetimes; only chemical production and/or loss (in the gaseous or aqueous phase) is considered in the predictions of their atmospheric abundances.

There are 41 gas-phase and twelve heterogeneous reactions in the background chemistry module applied to the 2D model grid. The scavenging of carbonaceous and sulfate aerosol species by precipitation is also included using a method based on a detailed 3D climate-aerosol-chemistry model (Wang 2004). Water vapor and air (N_2 and O_2) mass densities are computed using full continuity equations as a part of the atmospheric dynamics and physics model to which the chemical model is coupled. The climate model also provides wind speeds, temperatures, solar radiation fluxes and precipitation, which are used in both the global and urban chemistry formulations.

2.3.3 Coupling of Global and Urban Chemistry Modules

The urban chemistry module was derived based on an ensemble of 24-hour long CIT model runs and thus is processed in the IGSM with a daily time step, while the global chemistry module is run in a real time step with the dynamics and physics model, 20 minutes for advection and scavenging, 3 hours for tropospheric reactions. The two modules in the IGSM are processed separately at the beginning of each model day, supplied by emissions of non-urban and urban regions, respectively. At the end of each model day, the predicted concentrations of chemical species by the urban and global chemistry modules are then remapped based on the urban to non-urban volume ratio at each model grid. Beyond this step, the resultant concentrations at each model grid will be used as the background concentration for the next urban module prediction and also as initial values for the global chemistry module (Mayer *et al*. 2000).

2.4 Ocean Component

In the older IGSM1 (Prinn *et al*. 1999) a zonally averaged mixed layer ocean model with 7.8° latitudinal resolution was used. In the new IGSM2 the ocean component has been replaced by either a two-dimensional (latitude-longitude) mixed layer anomaly-diffusing ocean model (hereafter denoted as IGSM2.2) or a fully three-dimensional ocean GCM (denoted as IGSM2.3). Dalan *et al*. (2005b) showed that different versions of the 3-D ocean model with different rates of heat uptake can be produced by changing the vertical/diapycnal diffusion coefficients. However, changing the diapycnal coefficient also alters the ocean circulation, in particular the strength of North Atlantic overturning (Dalan *et al*. 2005a). Unfortunately it appears infeasible (certainly without changes to parameterizations in the 3-D models) to vary the heat uptake over the full range consistent with observations during the 20th century (Forest *et al*. 2008) and at the same time to maintain a reasonable circulation.

The ocean component of the IGSM2.2 consists of a Q-flux mixed layer model with horizontal resolution of 4° in latitude and 5° in longitude, and a 3000m deep anomaly diffusing ocean model beneath. The mixed layer depth is prescribed based on observations as a function of time and location (Hansen *et al*. 1983). In addition to the temperature of the mixed layer, the model also calculates the averaged temperature of the seasonal thermocline and the temperature at the annual maximum mixed layer depth (Russell *et al*. 1985). Diffusion in the deep ocean model is applied to the difference in the temperature at the bottom of the seasonal thermocline relative to its value in a present-day climate simulation (Hansen *et al*. 1984; Sokolov and Stone 1998). Since this diffusion represents a cumulative effect of heat mixing by all physical processes, the values of the diffusion coefficients are significantly larger than those used in sub-grid scale diffusion parameterizations in OGCMs. The spatial distribution of the diffusion coefficients used in the diffusive model is based on observations of tritium mixing into the deep ocean (Hansen *et al*. 1988). For simulations with different rates of oceanic heat uptake, the coefficients are scaled by the same factor in all locations.

The coupling between the atmospheric and oceanic components takes place every hour and is described by Kamenkovich *et al*. (2002) and Sokolov *et al*. (2005).

The mixed layer model also includes a specified vertically-integrated horizontal heat transport by the deep oceans, a so-called "Q-flux", allowing zonal as well as meridional transport. This flux is calculated from a simulation in which sea surface temperature (SST) and sea ice distribution are relaxed toward their present-day climatology with relaxation coefficient of 300 $W/m^2/K$, which corresponds to an e-folding time scale of about 15 days for a 100 m deep mixed layer. Relaxing SST and sea ice on such a short time scale, while being virtually identical to specifying them, avoids problems with calculating the Q-flux near the sea ice edge. The use of a two-dimensional (longitude-latitude) mixed layer ocean model instead of the zonally averaged one used in IGSM1 has allowed a better simulation of both the present day sea ice distribution and sea ice changes in response to increasing radiative forcing (Sokolov *et al*. 2005).

A thermodynamic ice model is used for representing sea ice. This model has two ice layers and computes ice concentration (the percentage of area covered by ice) and ice thickness.

The IGSM2.2 includes a significantly modified version of the ocean carbon model (Holian *et al*. 2001) used in the IGSM1. Formulation of carbonate chemistry (Follows *et al*. 2006) and parameterization of air-sea fluxes in this model are similar to the ones used in the IGSM2.3. Vertical and horizontal transports of the total dissolved inorganic carbon, though, are still parameterized by diffusive processes. The values of the horizontal diffusion coefficients are taken from Stocker *et al.* (1994), and the coefficient of vertical diffusion of carbon (K_{vc}) depends on the coefficient of vertical diffusion of heat anomalies (K_v). In IGSM1, K_{vc} was assumed to be proportional to K_v (Prinn *et al*. 1999; Sokolov *et al*. 1998). This assumption, however, does not take into account the vertical transport of carbon due to the biological pump. In the IGSM2.2 K_{vc} is, therefore, defined as:

$$K_{vc} = K_{vco} + rK_v \quad (1)$$

Since K_{vco} is a constant, the vertical diffusion coefficients for carbon have the same latitudinal distribution as the coefficients for heat. For simulations with different rates of oceanic uptake, the diffusion coefficients are scaled by the same factor in all locations. Therefore rates of both heat and carbon uptake by the ocean are defined by the global mean value of the diffusion coefficient for heat. In the rest of the paper the symbol Kv is used to designate the global mean value.

Comparisons with 3D ocean simulations have shown that the assumption that changes in ocean carbon can be simulated by the diffusive model with fixed diffusion coefficient, as used in the IGSM1, works only for about 150 years. On longer timescales the simplified carbon model overestimates the ocean carbon uptake. However, if Kvc is assumed to be time dependent, the IGSM2.2 reproduces changes in ocean carbon as simulated by the IGSM2.3 on multi century scales (Sokolov *et al*. 2007). Thus, for the runs discussed here, the coefficient for vertical diffusion of carbon was calculated as:

$$K_{vc}(t) = (K_{vco} + rK_v) \cdot f(t) \quad (2)$$

Where f(t) is a time dependent function constructed based on the analyses of the depths of carbon mixing in simulations with the IGSM2.3.

To evaluate the performance of the anomaly diffusing ocean model (ADOM) on different time scales Sokolov *et al*. (2007) carried out a detailed comparison of the results of simulations with the two versions of the IGSM2. Our results show that in spite of its inability to depict feedbacks associated with the changes in the ocean circulation and a very simple parameterization of the ocean carbon cycle, the version of the IGSM2 with the ADOM is able to reproduce the important aspects of the climate response simulated by the version with the OCGM through the 20th and 21st century and can be used to obtain probability distributions of changes in many of the important climate variables, such as surface air temperature and sea level, through the end of 21st century.

2.5 Global Land System

The Global Land System framework (GLS, Schlosser *et al*. 2007) integrates three existing models: the Community Land Model (CLM, e.g. Bonan *et al*. 2002), the Terrestrial Ecosystems Model (TEM, e.g. Melillo *et al*. 1993), and a Natural Emissions Model (NEM, Liu 1996). The GLS uses the CLM representation of the coupling of the biogeophysical characteristics and fluxes between the atmosphere and land (*e.g.*, evapotranspiration, surface temperatures, albedo, surface roughness, and snow depth). In addition, the CLM provides all of the hydrothermal states and fluxes (e.g., soil moisture, soil temperatures, evaporation, and precipitation events) at the appropriate spatial and temporal scales required by TEM and NEM. The TEM is then used to estimate changes in terrestrial carbon storage and the net flux of carbon dioxide between land and the atmosphere as a result of ecosystem metabolism. The NEM estimates the net flux of methane from global wetlands and tundra ecosystems and the net flux of nitrous oxide from all natural terrestrial ecosystems to the atmosphere. The sub-module in NEM describing processes leading to nitrous oxide emissions is primarily a globalization of the Denitrification Decomposition (DNDC) model of Li *et al*. (1992). Within the GLS, the algorithms of NEM that describe methane (CH_4) and nitrous oxide (N_2O) dynamics have been incorporated into TEM so that TEM now describes the hourly and daily dynamics of these trace gases in addition to the monthly dynamics of carbon dioxide and organic matter in terrestrial ecosystems. The direct coupling between these two models allows monthly TEM estimates of reactive soil organic carbon to determine nitrous oxide fluxes. In addition, a new procedure has been developed that provides a statistical representation of the episodic nature and spatial distribution of land precipitation. This is required for two reasons: 1) an "episodic" provision of zonal precipitation from the IGSM's atmospheric sub-model represents more realistic hydrologic forcing to CLM than a constant precipitation rate applied at every time step for every zonal band, and 2) the N_2O module of NEM requires precipitation events that vary in intensity and duration along with corresponding dry periods between storm events to employ its decomposition, nitrification, and denitrification parameterizations.

All land areas across the globe are assumed by TEM and NEM to be covered by natural vegetation, which is held constant in time. To match and couple with the zonal configuration of the atmospheric dynamics and chemistry, the areas for each land cover type at the native 0.5^{o}

latitude x 0.5^o longitude grid cells (employed by both CLM and TEM) have been aggregated within each 4^o latitudinal band used by the atmospheric dynamics and chemistry model (Schlosser *et al*. 2007). Thus, each latitudinal band represents a 4^o latitude x 360^o longitude grid cell in the GLS framework. The GLS is run for all land cover types found in these zonal cells and the area covered by each land cover type is used to determine the relative contribution of that land cover type to the zonally aggregated water, energy, carbon and nitrogen fluxes from the terrestrial systems. As shown by Schlosser *et al*. (2007), the zonal fluxes from GLS are not substantially affected by the implementation the of zonal mosaic land cover data in the IGSM2 as compared to their performance using explicit latitude/longitude grids. The timing and location of the carbon sink sand source regions is preserved, and the spatiotemporal patterns of evapotranspiration agree well with a consensus of state-of-the-art biogeophysical models as determined by the Global Soil Wetness Project Phase 2 (GSWP2, Dirmeyer *et al*. 2002). Moreover, one of the more desirable changes in the patterns of carbon flux by TEM in the zonal GLS configuration, as compared to a previous version of TEM employed in the IGSM, is the removal of an erroneous, mid-summer carbon emission at northern high latitudes, which is not seen in spatially explicit TEM simulations forced by observed atmospheric conditions (refer to Schlosser *et al*. 2007, for more details).

In TEM, the potential uptake of atmospheric CO_2 by plants is assumed to follow Michaelis-Menten kinetics, according to which the effect of atmospheric CO_2 at time t on the assimilation of CO_2 by plants is parameterized as follows:

$$f(CO_2(t)) = (C_{max}\, CO_2(t)) / (kc + CO_2(t)) \quad (3)$$

where C_{max} is the maximum rate of C assimilation, and *kc* is the CO_2 concentration at which C assimilation proceeds at one-half of its maximum rate (*i.e*. C_{max}). The sensitivity of plant uptake on *kc* is defined not by the absolute value of $f(CO_2(t))$, which decreases with *kc,* but by the ratio of $f(CO_2(t))$ to $f(CO_2(0))$ which increases with *kc*. This ratio can be approximated as $1+\alpha\log(CO_2(t)/ CO_2(0))$. In contrast to most of the terrestrial biosphere models currently used in climate change assessments (Plattner *et al*. 2008), TEM takes in to account nitrogen limitations on net carbon storage. This significantly decrease sensitivity of the terrestrial carbon uptake to the increase in the atmospheric CO_2 concentration and affect sign of the feedback between terrestrial carbon cycle and climate (Sokolov *et al*. 2008a).

3. METHODOLOGY

3.1 General approach for making projections

The basic method we employ for uncertainty analysis is Monte Carlo simulation, in which multiple input sets are sampled from probability distributions representing uncertainty in input parameters. Pure random sampling typically requires many thousands of samples to converge to a stable distribution of the model output. Therefore, a number of alternative more efficient sampling strategies have been developed. In this study, we use Latin Hypercube Sampling (LHS) (Iman and Helton 1988). LHS divides each parameter distribution into *n* segments of equal probability, where *n* is the number of samples to be generated. Sampling without

replacement is performed so that with *n* samples every segment is used once. We use a sample size of 400 for each s simulation ensemble.

3.2 Physical/scientific uncertainties

3.2.1 Climate sensitivity, mixing of heat into the ocean, and aerosol forcing

Three properties that are commonly recognized as being major contributors to the uncertainty in simulations of future climate change are the effective climate sensitivity of the system (S), the rate at which heat is mixed into the deep ocean (Kv), and the strength of the aerosol forcing associated with a given aerosol loading (Faer) (Meehl *et al*. 2007a). These same properties and their uncertainties also affect 20th century simulations. Thus in principle estimates of these properties and their uncertainties can be derived from simulations in which these properties are varied to determine which give simulations consistent with observed 20th century changes.

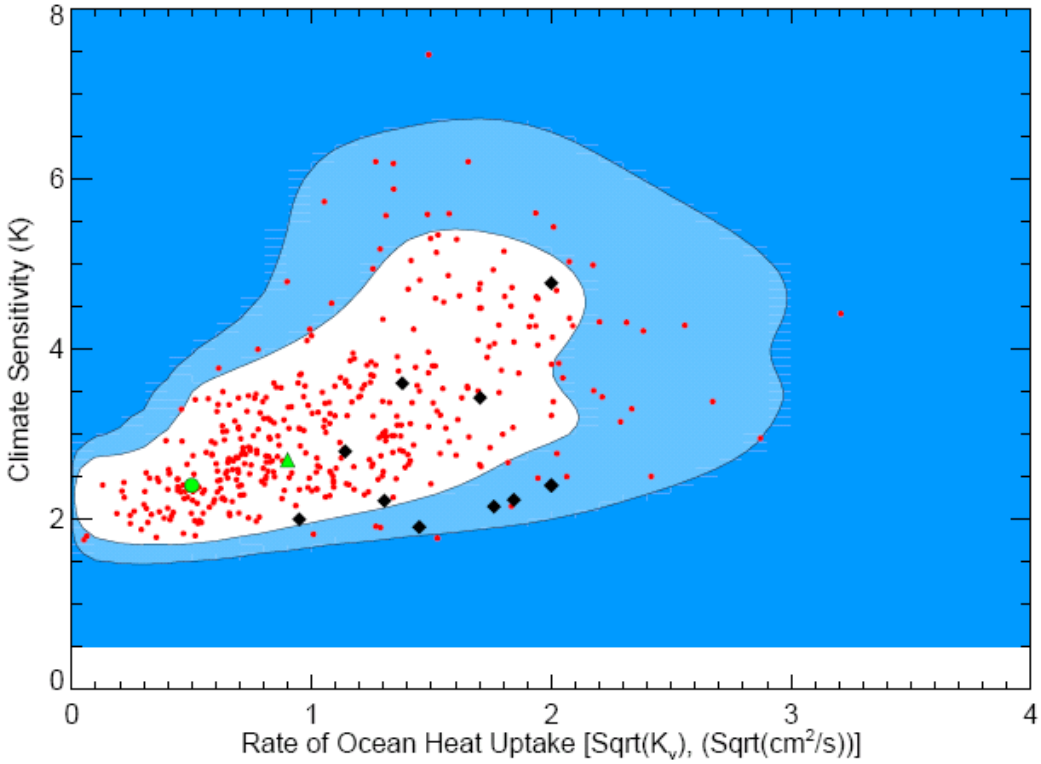

Figure 2. The marginal posterior probability density function for S-Kv parameter space. The shading and thick contours denote rejection regions for significance levels of 10% and 1% respectively. Green circle and triangle indicate mode and a median on the distribution respectively. Black diamonds indicate values of the parameters of the MIT climate model needed to represent behavior of different AR4 AOGCMs in the simulations with 1% per year increases in the CO_2 concentration. Red dots show values for Kv and S from 400 samples.

In the present study, we use the probability distribution functions (pdfs) estimated in this way by Forest *et al*. (2008). The values of S, Kv, and Faer were varied systematically in the climate model component of the IGSM and a large ensemble (~600) of simulations of 20th century

climate was carried out. The simulations were compared against observations of surface, upper-air, and deep-ocean temperature changes. For each diagnostic the likelihood that a given simulation is consistent with the observed changes, allowing for observational error and natural variability, was estimated using goodness of fit statistics from climate change detection methods (see Forest *et al*. 2002, 2006, 2008). By combining the likelihood distributions estimated from each diagnostic using Bayes' Theorem, a *posterior* probability distribution was obtained. As with other estimates of probability distributions using Bayesian methods, *priors* on the three parameters are required. For climate sensitivity, the *prior* distribution was calculated by Webster and Sokolov (2000) from an expert elicitation by Morgan and Keith (1995). This *prior* essentially limits the possible climate sensitivities to being less than 7 ^{o}C, consistent with expert opinion (Webster and Sokolov 2000; Hegerl *et al*. 2007). Uniform distributions were used as priors for the other two parameters.

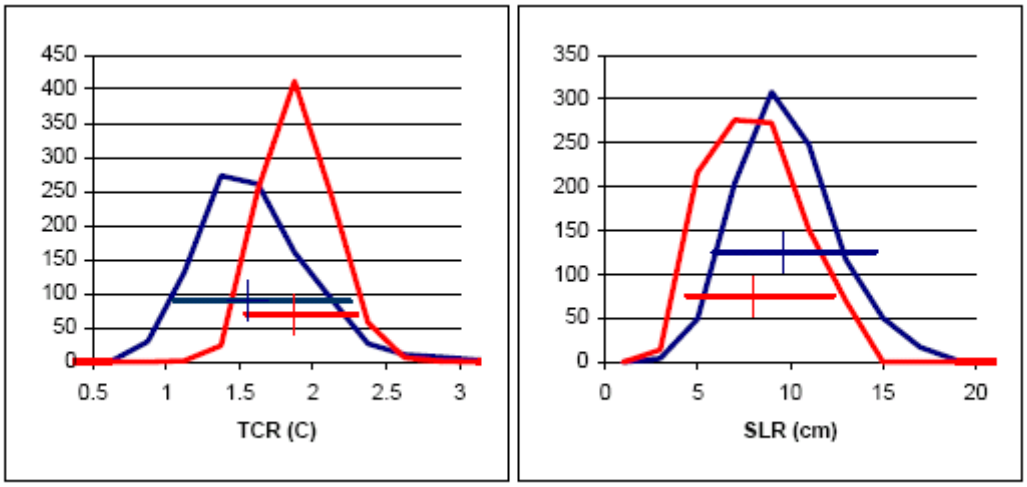

Figure 3. Frequency distributions for changes in surface air temperature and thermosteric sea level rise averaged over years 61-80 in simulations with 1% per year CO_2 increase, obtained from the fits for the IGSM1 (blue) and IGSM2.2 (red) using climate parameter distributions from Forest et al., (2002) and Forest et al. (2008), respectively.

The resulting two-dimensional marginal distribution for effective climate sensitivity and the rate of deep-ocean heat uptake is shown in **Figure 2**, along with the locations in this parameter space of 10 AOGCMs (estimated from data in the CMIP3 archive (Meehl *et al*. 2007b). The joint distribution differs significantly from the earlier distribution, developed in Forest *et al*. (2002) and used in Webster *et al*. (2003), because the model simulations for the twentieth century used by Forest et. al. (2006 and 2008) include several additional forcings. Most importantly they include stratospheric aerosols from volcanic eruptions and, because these caused a cooling in the latter half of the 20th century, higher climate sensitivities and lower rates of ocean heat uptake are required to match the observed temperature changes. The effect of these shifts in the probability distribution can be summarized in the likelihood distribution for changes in surface air temperature and thermosteric sea level rise due to CO_2 increase at 1% per year rate (**Figure 3**). The higher lower bound for TCR and lower upper bound for sea level rise

are a direct result of the shift in the distributions for climate sensitivity (S) and the effective thermal diffusivity (Kv).

The LHS sampling method used in Webster *et al*. (2003) generated samples for Kv, S and Faer from their individual 1D marginal pdfs, and imposed the correlation structure of the joint 3D pdf on the samples. In contrast, now after picking a Kv sample from the 1D marginal pdf, we generate a 2D pdf for S and Faer conditional on the chosen Kv value, and then calculate a 1D marginal pdf for S from that 2D pdf, and sample the new pdf for S. Finally, we generate a 1D pdf for Faer conditional on the two chosen values of Kv and S , and sample that pdf for a value of Faer. This new sampling strategy preserves the uniqueness of the samples by not allowing one to choose from the same bin number in the conditional pdfs, though it theoretically may sample the same value of S or Faer few times in contrast to the earlier method. New method better preserves the full details of the original three dimensional pdf. Values for Kv and S from the 400 samples are shown on Figure 2 by red dots.

3.2.2 Uncertainty in carbon cycle

As described in section 2.4, the vertical diffusion coefficient for carbon depends on the effective vertical diffusivity for temperature anomalies, Thereby uncertainty in carbon uptake by the ocean is linked to the uncertainty in heat uptake. Values of the parameters in the equation for Kvc (Eq. 1) were estimated so that, for the range of Kv, deduced from observations, the oceanic carbon uptake for the 1980s spans the observed uncertainty range given in the IPCC TAR. The values of Kvco and r that satisfy this requirement are 1.0 $cm^2\ s^{-1}$ and 3.0 respectively.

In contrast to Webster *et al*. (2003), in the present study, we take into account uncertainty in the fertilization effect of atmospheric CO_2. The results of CO_2-enrichment studies suggest that plant growth could increase from 24% to 50% in response to doubled CO_2 given adequate nutrients and water (Raich *et al*. 1991; McGuire *et al*. 1992; Gunderson and Wullschleger 1994; Curtis and Wang 1998; Norby *et al*. 2005). In TEM, a value of 400 ppmv CO_2 is normally chosen for the half-saturation constant *kc* (Eq. 3) so that $f(CO_2(t))$ increases by 37% for a doubling of atmospheric CO_2 from 340 ppmv to 680 ppmv CO_2 (McGuire *et al*. 1992, 1993, 1997; Pan *et al*. 1998). A 24% response to doubled CO_2 would correspond to a *kc* value of 215 ppmv CO_2 whereas a 50% ppmv CO_2 response would correspond to a *kc* value of 680 ppmv CO_2, for the same changes in atmospheric CO_2. As these enrichment studies may not have covered the full range of uncertainty, we used 150 ppmv as a low bound for *kc* and 700 ppmv as the upper limit.

3.2.3 Precipitation frequency

Another physical uncertainty in the coupled earth system model is how the frequency of precipitation changes with increases in surface temperature. Changes in mean precipitation (over space and time) are fundamentally a result of shifts in the character of individual precipitation events, which are determined by the frequency at which they occur as well as their (expected) duration and intensity. It is these quantities that, in large part, determine the hydrologic climate of any region (i.e. the partitioning of precipitation between evaporation and runoff) as well as the

ecology and biogeochemistry of the ecosystems. For example, more runoff results in greater flood potential, less water infiltration into the soils and less storage available to plants, as well as fewer saturating events that can impede nitrous oxide emissions (from soils) as well as methane-emitting environments. Such responses to climate change can have substantial consequences on natural and managed terrestrial systems, as well as providing potentially strong feedback mechanisms to the rest of the climate system. We therefore introduce an approach that provides a probability-based extrapolation of precipitation frequency change associated with climate warming.

Lacking observations adequate for estimating this trend, we use the results of the AOGCMs that participated in the IPCC AR4 to develop probability distributions of the trend. From the model archive, we consider the pre-industrial control runs and the transient CO_2 doubling runs, in which the daily outputs of precipitation are archived for at least a 20-year period. For every grid point of the GCMs' time series, we determine for each day whether or not the model produced a sufficient amount of precipitation to be construed as a "wet" day. In doing so, our calculations require a threshold value for the daily precipitation rate of a grid cell above which we deem a precipitation "event" has occurred for that day. For this threshold we have chosen 2.5 mm/day (see Schlosser and Webster, 2008 for details). From this, we determine for each month of the simulation period the total number of days that a precipitation event occurred, and subsequently the average number of days between "wet" days for the month. To obtain a representative monthly climatology of these precipitation intervals, we calculate these statistics for each month, for every grid cell, and average them over the 20-year period for the pre-industrial runs as well as the transient run, the latter centered at the time of doubling of CO_2. Then, by taking the difference in these monthly constructions of precipitation interval, we can make an inference as to any particular GCM's propensity to change under forced climate change (i.e. to a doubling of CO_2 concentrations). Then, to configure these results to the IGSM zonal atmospheric structure, these gridded results are averaged over each of the GCMs' latitude bands, and then pooled into latitudinal regions with common statistical traits (i.e. sign, magnitude, etc.) that correlate well with the large-scale circulations and precipitation patterns. Once obtained, these (simulated) changes in this derived hydrologic diagnostic are associated with each AOGCM's change in global temperature. Thus, the zonally-averaged changes in precipitation interval from each AOGCM are normalized according to their global temperature change.

Once we have calculated these pooled, zonally-averaged normalized changes in precipitation interval, based on the AR4 AOGCMs, we fit probability density functions to the distributions from the models. Each zonal band has a probability distribution of temperature-dependent trends, but additionally we impose correlation across zonal groups to reflect the observed correlations in the AOGCM results. As with other uncertain parameters, we perform Latin Hypercube sampling from these distributions, while imposing the observed zonal correlation structure within samples.

3.3 Economic/emissions uncertainties

The uncertainty in the emissions of all greenhouse gases and pollutants are taken from an uncertainty analysis of the Emissions Projection and Policy Analysis model (Paltsev *et al*. 2005). This analysis is summarized briefly here; see Webster *et al* (2008) for more detail. Compared with previous efforts (Webster *et al*. 2002 and 2003) several aspects of the EPPA model and of the uncertainty analysis have been improved. The technological detail of the model has been deepened, with the explicit representation of private automobiles, commercial transportation, and the service sector and the addition of biofuels as a low carbon alternative in transportation.

The characterization of emissions coefficients for pollutants was substantially changed. Whereas in previous versions of EPPA we relied on a Kuznets curve approach, the specification now used in the Monte Carlo analysis estimates an advancing technological frontier and catch-up to this frontier by lagging regions. Statistical work by Stern (2006 and 2005) has suggested this approach better represents the process. Also, the specification of uncertainty in economic growth has been substantially revised. Rather than sampling high or low growth rates that applied to the 100 year horizon as has been done previously in most Monte Carlo studies of emissions, we created stochastic growth paths characterized as a random walk where the uncertainty was estimated for each region/country for the period 1950-2000. As a result, regions experience periods of boom and bust over the 100 year horizon like that which characterized growth in the latter half of the last century rather than smooth growth that was either fast or slow.

These new approaches for representing uncertainty in productivity growth and in emissions coefficients allowed us to draw more directly from historical data to estimate uncertainty distributions rather than to rely on expert judgment, and to simulate growth patterns that varied across regions and over time that are more realistic. The new approach to simulating uncertainty in growth of gross domestic product (GDP) has narrowed the distribution of outcomes because regional growth rates are uncorrelated with each other. The result is that range of possible growth for individual regions is wide, but the global range is narrower as statistically rapid growth in some regions is likely to be offset by slow growth in other regions. The new approach on emissions coefficients for other pollutants results in lower median emissions of pollutants like SO_x, NO_x, and CO.

Uncertainty in emissions were developed from the EPPA model using the same Latin Hypercube Sampling approach employed here, creating a 400 member ensemble to match to match the 400 sample sets for the earth system model components (Webster *et al*.2008). Each of these 400 EPPA simulations provides a set of emissions for all pollutant species that are consistent: to the extent that emissions of different species derive from the same combustion sources (*e.g.*, oil, gas, coal) they are each consistent with the amount of fuel combusted given uncertainty in emissions per unit of fuel. Each emission set is then considered to be one emissions sample that is paired randomly with one set of values for the climate parameters following the LHS protocol of sampling without replacement.

3.4 Design of the simulations

The estimates of changes in climate variables presented below are obtained from the 400 member ensemble of climate change simulations with different values of the uncertain input parameters. Because of the large inertia of the ocean and carbon reservoirs, each simulation starts in 1861 and is conducted in two stages: a simulation with historical forcings and a future climate projection. During the first stage, from 1861 to 1990, the model is forced by the observed changes in GHG concentrations (Hansen *et al*. 2002), tropospheric and stratospheric ozone (Wang and Jacob 1998), the solar constant (Lean 2000), sulfate aerosols (Smith *et al*. 2004), and volcanic aerosols (Sato *et al*. 1993). For this stage, different sets of values of the climate sensitivity, the rates of oceanic heat and carbon uptakes, total aerosol forcing, the strength of CO_2 fertilization and changes in precipitation frequency are used in each simulation.

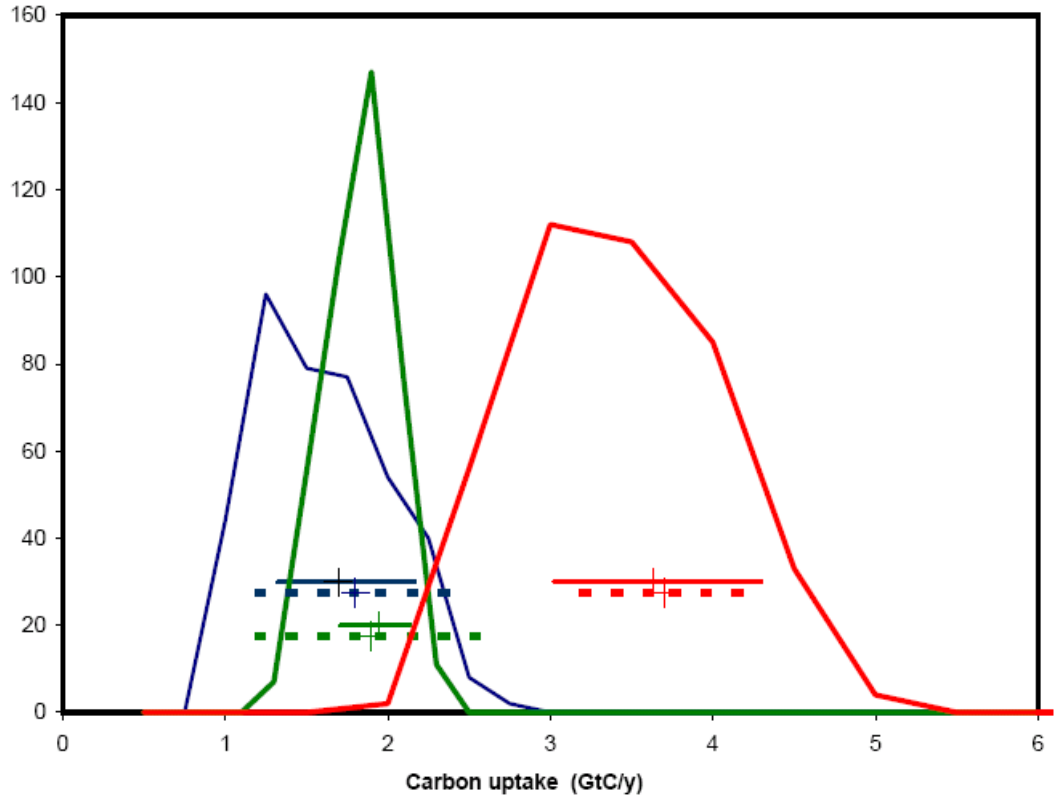

Figure 4. Frequency distributions for carbon uptake by ocean (blue), terrestrial ecosystem (green) and total (red) averaged over 1980s. Solid horizontal bars show 5-95% ranges from 400-member ensemble of simulations with the MIT IGSM, dashed horizontal bars show 5-95% ranges from the IPCC TAR.

To simulate changes in oceanic and terrestrial carbon stocks, the ocean carbon model and TEM are forced by the observed changes in atmospheric CO_2 concentration and simulated climate. While uncertainties in ocean carbon diffusion and strength of CO_2 fertilization do not affect atmospheric CO_2 concentrations and associated climate during this historical period, they do affect carbon uptakes by land and ocean and, therefore, changes in corresponding carbon stocks. In the simulations described by Webster *et al*. (2003) carbon uptake by terrestrial

ecosystem was adjusted to balance carbon cycle for the 1980s. No such adjustment is used in the present study. The resulting frequency distributions for the terrestrial, oceanic and total carbon uptake are shown **Figure 4**. Our ranges of carbon uptake by the ocean and the terrestrial ecosystem are somewhat narrower than those given in the IPCC TAR. However the distribution for the total uptake is rather wide with a 90% range from 2.1 to 4.0 GtC/year.

In the second-stage of the simulations, which begins in 1991, the full version of IGSM2 is forced by emissions of greenhouse gases and aerosol precursors. Historical emissions are used through 1996 and emissions projected by the EPPA model from 1997 to 2100. In this future climate stage of the simulations, concentrations of all gases and aerosols are calculated by the atmospheric chemistry sub-model based on anthropogenic and natural emissions and the terrestrial and oceanic carbon uptake provided by the corresponding sub-components. In these simulations changes in concentration of black carbon aerosol are explicitly calculated. Since they were not considered in the preceding stage, the total aerosol forcing assumed in the first stage was adjusted to take the black carbon contribution into account. Uncertainties in the economic factors that affect anthropogenic emissions are taken into account in addition to climate related uncertainties.

To evaluate the contributions to the total uncertainty in the projected climate changes due to the separate uncertainties in emissions and climate characteristics, we carried out two additional 400 member ensembles of simulations that each includes the uncertainties from just one of these two sources. In the first set of simulations the median values of the climate parameters were used while the uncertainty in the emissions was included, and in the second the median values of the emissions were used while the uncertainty in the climate parameters was included.

4. 21st CENTURY PROJECTIONS OF ANTHROPOGENIC CLIMATE CHANGE

In section 4.1 we present and discuss the projections of the levels of all the important greenhouse gases and aerosols that contribute to radiative forcing of climate change. The forcing and related changes in climate are discussed in section 4.2, together with the contributions of economic and scientific uncertainties to the uncertainty in projected climate. Changes in the biogeochemical cycles of carbon dioxide, nitrous oxide and methane that are influenced by the joint effects of chemistry, biology and climate change are discussed in section 4.3. In section 4.4 our projections are compared with the results of the IPCC AR4. Sensitivity of our projections to the uncertainty in the estimates of the 20th century changes in deep ocean heat content are discussed in section 4.5.

4.1 Greenhouse gas projections

Figure 5a shows (in red) the projections of the median and 95% range for CO_2 mole fractions. Compared to our earlier projections (shown in blue), the new projections are significantly higher due in part to higher projected CO_2 emissions (see section 3.3) and in part to changes in the oceanic and land sinks (see section 4.3 for further discussion).

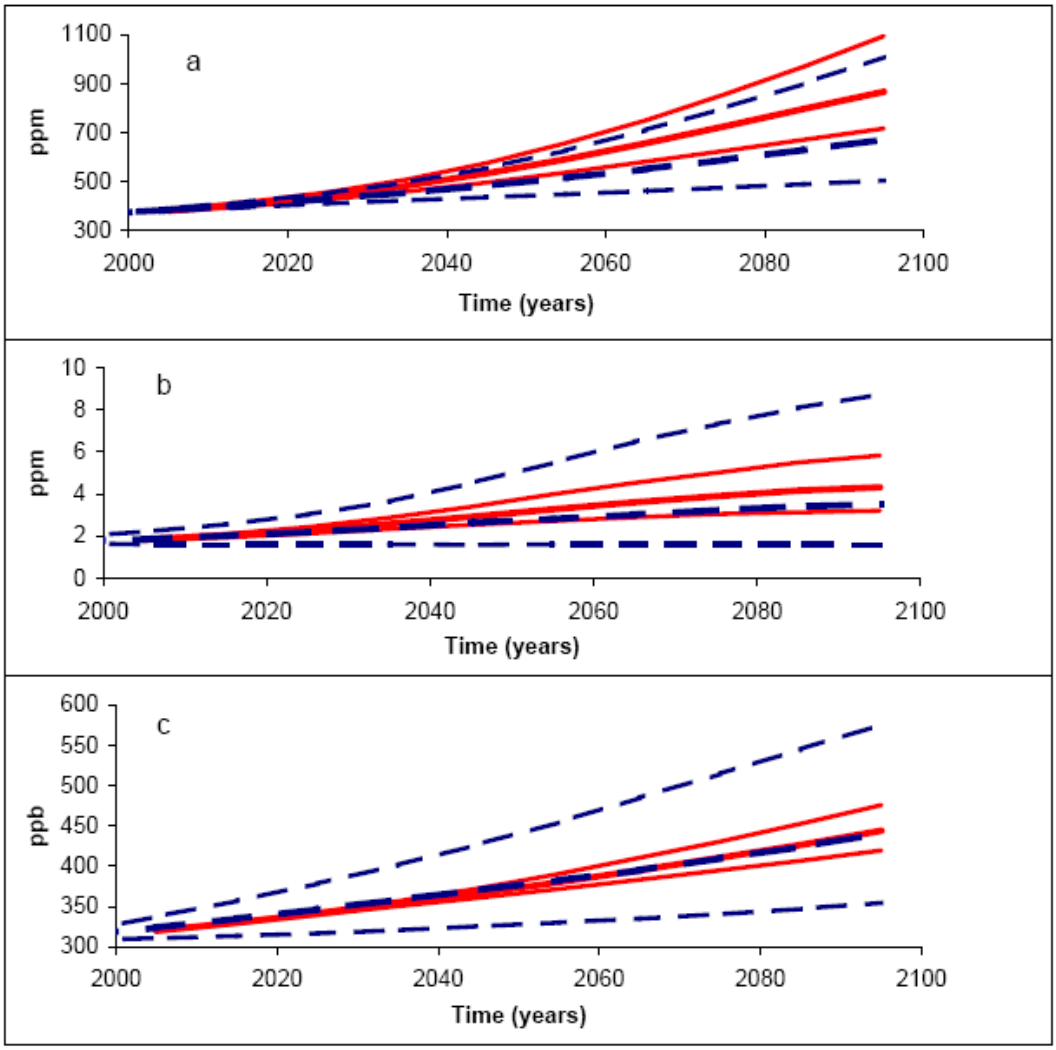

Figure 5. Projected decadal mean concentrations of CO_2 (a), CH_4 (b), and N_2O (c). Red solid lines are median, 5% and 95% percentiles for present study: dashed blue line the same from Webster et al. (2003).

For CH_4, the current median projections are very similar to the previous ones but the 95% range has decreased by almost a factor of three (**Figure 5b**). This is due in part to a lowered range in CH_4 emissions (section 3.3) but also to a decrease in the range of projected OH concentrations (**Figure 6b**). The projected median 24% decrease in OH by 2100 results from the effects of the projected increases then decreases of NOx, which produces OH, being offset by the projected CH_4, CO and VOC increases (all of which remove OH). The projections of NO_x, CO and VOC concentrations are closely correlated with their emissions, which are shown in Webster *et al*. (2008).

For the significant greenhouse gas ozone (O_3), the projected mole fractions increase through 2050 but then decrease after that (red curves in **Figure 6a**). This is driven significantly by the projected post-2050 decrease in NO_x. Ozone mole fractions increase the most when CO, VOC

and NO_x mole fractions all increase together, but not when CO and VOC increases accompany NO_x decreases.

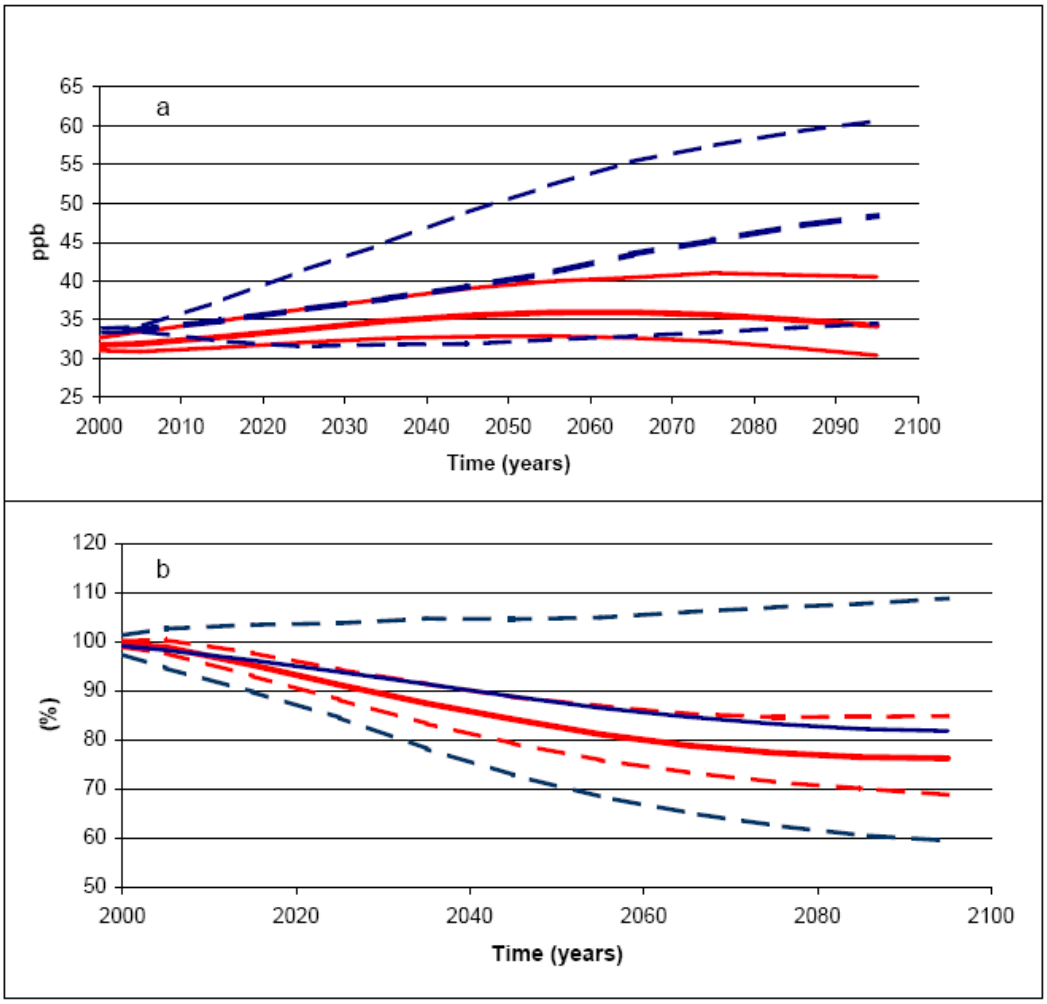

Figure 6. Projected decadal mean concentrations of ozone (a), and OH radical (b). The latter is shown as a ratio to its values averaged over years 1991-2000. Red solid lines are median, 5% and 95% percentiles for present study: dashed blue line the same from Webster et al. (2003).

Median nitrous oxide (N_2O) mole fractions are projected to increase by about 50% by 2100 (**Figure 5c**) driven by increasing anthropogenic emissions (section 3.3) and increased natural emissions induced by projected increase in soil temperature, rainfall and soil labile carbon.

Projected mole fractions of the "industrial" gases listed in the Kyoto Protocol are shown in **Figure 7** (hydrofluorocarbons, HFCs, aggregated; perfluorocarbons, PFCs, aggregated; sulfur hexafluoride). The trends and uncertainties in these long-lived gases, which have very large GWPs, are dominated by the trends and uncertainties in their projected emissions, but augmented in the case of the HFCs by the negative trend and uncertainty in their major sink OH (Figure 6b).

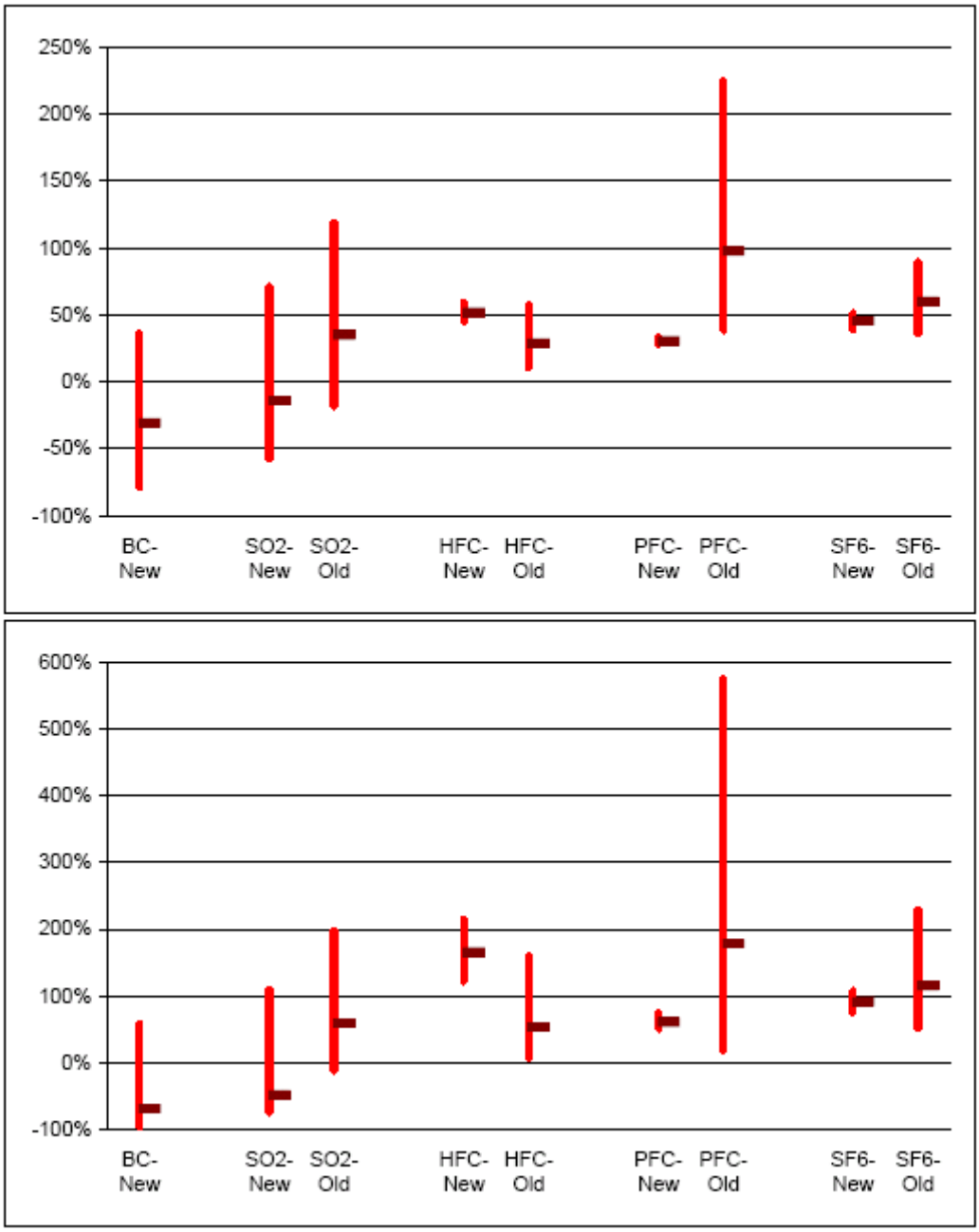

Figure 7. Changes in concentration of some GHGs averaged over 2041-2050 (a) and 2091-2100 (b) relative to 1991-2000 in present study (new) and in Webster et al., (2003) (old). HFCs and SFC are reduced by factors 100 and 10, respectively. Radiative effect of changes in the concentration of black carbon was not taken into account in Webster et al. (2003).

Figure 7 also shows projections of mole fractions of SO_2, which is the precursor for sulfate aerosols and has both anthropogenic and natural (dimethyl sulfide oxidation) sources. The median and range projections are driven primarily by the projected anthropogenic emissions, but augmented by the projected decrease and uncertainty in OH, which is the principal gas-phase sink for SO_2 (converting it to sulfate aerosol).

Finally, black carbon projections are also shown in Figure 7. Like the SO_2 projections, they are driven by the anthropogenic emissions but are not affected by OH. Their principal removal is instead through dry and wet deposition to the surface.

4.2 Projected changes in climate

As a result of the changes in concentrations of GHGs and sulfate and black carbon aerosols described in section 4.1, by the end of the 21st century radiative forcing will increase between 6.2 W/m^2 and 9.8 W/m^2 (90% range) compared to the year 1990, with a median increase of 7.9 W/m^2 (**Figure 8a**).

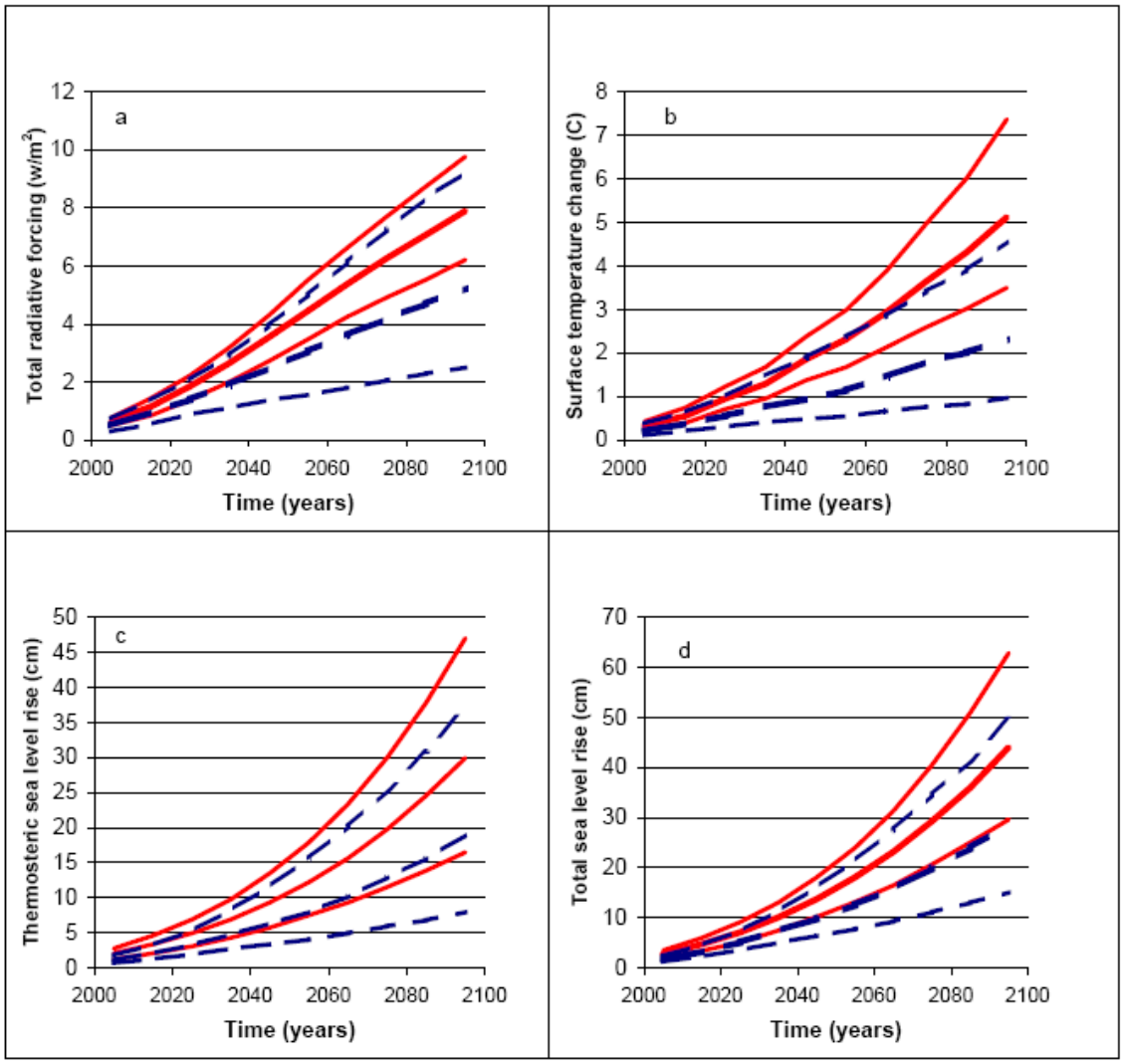

Figure 8. Projected changes in decadal mean radiative forcing (a), surface air temperature (b), sea level rise due to thermal expansion (c) and total sea level rise (d). Red solid lines are median, 5% and 95% percentiles for present study: dashed blue line the same from Webster et al. (2003).

Changes in GHG emissions and carbon uptake lead to a significant increase of both the lower bound of the 90% range and also the median forcing compared to the results of Webster *et al.* (2003). The probability of the radiative forcing being less than 5.0 W/m^2 is about 45% according

to Webster at al. (2003) but less than 1% according to our new study. At the same time the upper bounds of the 90% ranges differ by only 0.6 W/m^2 between the two studies. In fact the new upper 90% bound on the forcing due to GHGs (**Table 1**) only is even lower than the one in Webster *et al*. (2003). The slightly higher value of the upper 90% bound for the total forcing is a result of different changes in sulfate aerosol loading and the fact that forcing associated with changes in black carbon aerosol was not taken into account by Webster *et al*. (2003). The total forcing includes contributions from changes in GHGs, sulfate aerosol, tropospheric ozone as well as, in present study, black carbon. As shown in section 3.2, use of the revised probability distributions for the climate parameters leads to larger surface warming and smaller thermal expansion of the ocean for a given forcing (Figure 3). This effect together with the differences in radiative forcing described above result in a significantly higher increase in SAT (**Figure 8b** and Table 1) than was projected by Webster *et al*. (2003). While the upper 90% bound for surface warming projected in this study is noticeably larger than in Webster *et al*. (2003), (7.4^{o}C instead of 4.6^{o}C), the changes in the lower part of the projected range are even more significant. According to Webster *et al*. (2003) there was a 40% probability of SAT increasing by less than 2^{o}C by the end of 21st century relative to 1990 for the "business-as-usual" emissions scenario, in the present study surface warming exceeds 2^{o}C in all 400 simulations. We will compare our projections of possible climate change with projections given in the IPCC AR4 in section 4.4.

Table 1. Distributions of CO_2 concentration, radiative forcing, changes in surface air temperature, thermosteric sea level rise and sea level rise due to thermal expansion and glacial melt.

Variable	Ensemble	Time	5%	Median	95%
	Present study	2045	495	533	574
CO_2	Webster et al. 2003		434	483	554
(ppmv)	Present study	2095	716	866	1095
	Webster et al. 2003		502	670	1013
Radiative	Present study	2045	2.73	3.27	3.86
forcing	Webster et al. 2003		1.36	2.51	4.23
due to GHGs	Present study	2095	5.98	7.54	9.40
(W/m^2)	Webster et al. 2003		2.33	5.48	9.80
Total	Present study	2045	2.71	3.53	4.28
radiative	Webster et al. 2003		1.38	2.47	3.95
forcing	Present study	2095	6.21	7.89	9.77
(W/m^2)	Webster et al. 2003		2.50	5.22	9.21
	Present study	2045	1.37	1.85	2.37
SAT	Webster et al. 2003		0.57	1.34	1.80
(^{o}C)	Present study	2095	3.50	5.12	7.37
	Webster et al. 2003		1.03	2.37	4.61
Thermosteric	Present study	2045	6	9	14
sea level	Webster et al. 2003		3	6	12
rise	Present study	2095	16	30	47
(cm)	Webster et al. 2003		8	19	37
Total	Present study	2045	10	14	18
sea level	Webster et al. 2003		6	10	14
rise	Present study	2095	29	44	63
(cm)	Webster et al. 2003		15	29	50

From the above mentioned decrease in the thermal expansion of the ocean for a given forcing (Figure 3b) and the similarity of the upper 90% bounds of forcing (Figure 8a), one might expect the upper limit of the thermosteric sea level rise to be smaller in the present study than in Webster *et al*. (2003). However, this is not the case[1] (**Figure 8c**). This apparent contradiction is explained by the changes in the ocean carbon model. As shown by Sokolov *et al*. (1998), the assumed dependency between rates of heat and carbon uptake by the ocean imposes a negative correlation between the rate of heat mixing into the deep ocean and the atmospheric CO_2 concentration, which leads to a decrease in the uncertainty range for thermal expansion. Changes in the parameterization of oceanic carbon uptake in the current model (see section 2.3 and Sokolov *et al*. 2007) weakened this correlation, resulting in a wider range of the thermosteric sea level rise. The differences between the two studies in projected sea level rise, especially in the component related to the thermal expansion of the deep ocean, are, however, relatively smaller than the differences in projected surface temperature (Figure 8).

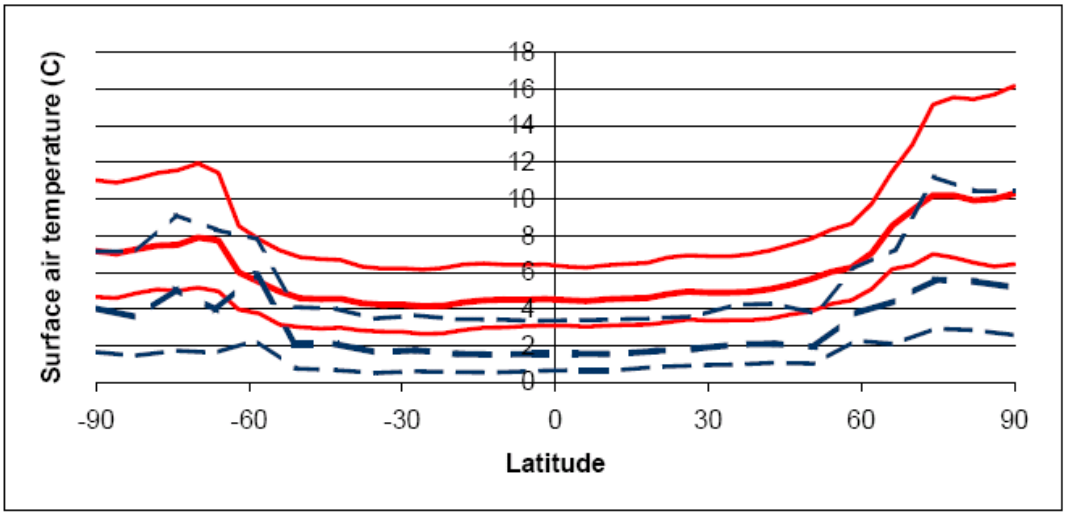

Figure 9. Latitudinal distribution of changes in SAT in the last decade of 21st century relative to 1981-2000. Red solid lines are median, 5% and 95% percentiles for present study: dashed blue line the same from Webster et al. (2003).

The latitudinal pattern of increases in SAT (**Figure 9**) is similar to those simulated by coupled AOGCMs, with polar amplification being larger in the Northern Hemisphere. Asymmetry in surface warming between the two hemispheres increases in time (**Figure 10**). As can be expected changes in SAT in polar regions are highly correlated with changes in sea ice cover (not shown). According to our simulations there is a 5% probability of the Arctic Ocean becoming ice free during summer and 1% probability of its becoming ice free for the whole year by the end of the century. In 1% of the simulations summer sea ice disappears by the year 2085. In the Southern Hemisphere the sea ice, while significantly decreasing, remains present in all simulations during the whole year.

[1] Due to an error in the postprocessor, values of thermosteric sea level rise shown in Webster et al. (2003) are about 50% larger than they really were.

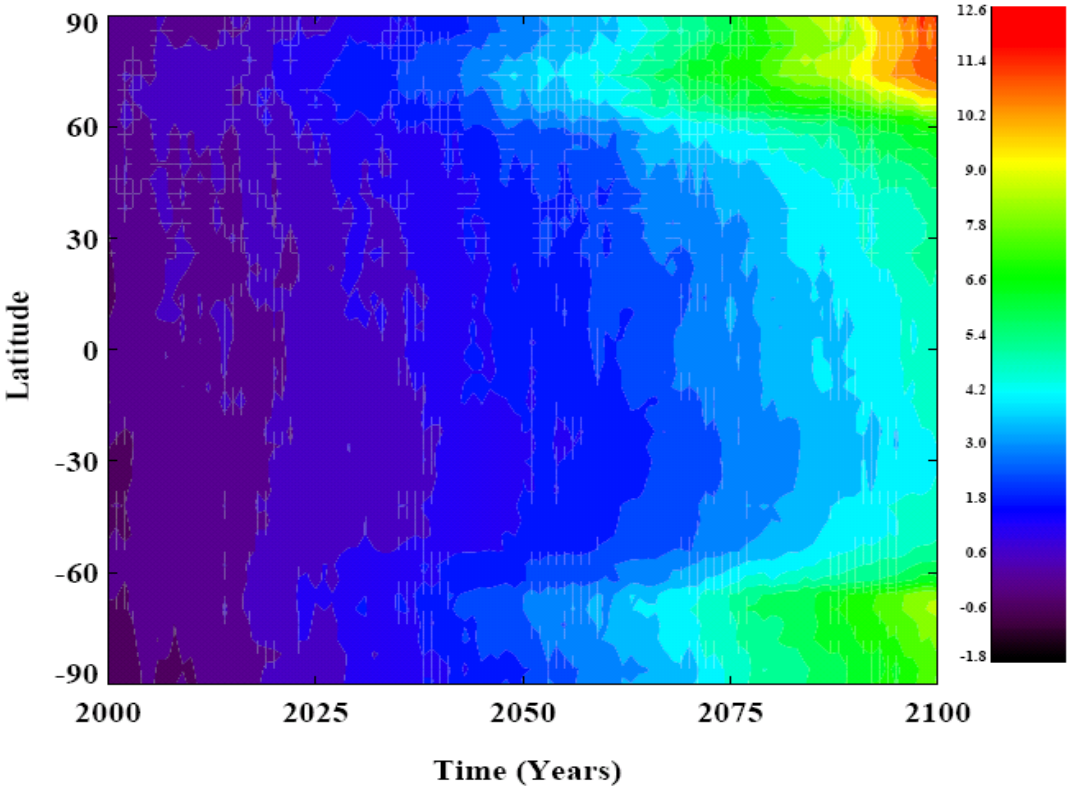

Figure 10. Transient change in surface air temperature in simulation with median values of parameters for both economics and climate models.

As indicated in section 3.4, we carried out two additional ensembles of simulations aimed at estimating the relative contributions of economics and climate uncertainties to the uncertainties in the projected climate change. As could be expected, uncertainties in atmospheric CO_2 concentration and radiative forcing (**Figures 11a and 11b**) are primarily related to the uncertainties in emissions, with a small contribution from uncertainties in the carbon uptake by land and ocean. Ignoring uncertainties in the behavior of climate system leads to an overestimation of the lower 90% bound and the median, but does not affect the upper 90% bound of the range of projected surface warming (**Figure 11c**). Nevertheless, uncertainties in surface air temperature associated with the uncertainties of input parameters from the two different sources are rather similar (see **Table 2**).

Table 2. Ratios of the percentiles to mean values for distributions of surface warming and sea level rise at the last decade of 21st century in ensembles with full, climate and emission uncertainties.

SAT	**5%**	**16.7%**	**50%**	**83.3%**	**95%**
Full uncertainty	0.66	0.78	0.97	1.22	1.40
Climate uncertainty	0.74	0.82	0.99	1.17	1.35
Emission uncertainty	0.75	0.85	0.99	1.16	1.25
Sea level rise	**5%**	**16.7%**	**50%**	**83.3%**	**95%**
Full uncertainty	0.64	0.76	0.98	1.24	1.43
Climate uncertainty	0.67	0.80	0.98	1.20	1.36
Emission uncertainty	0.82	0.88	1.00	1.12	1.19

In the case of sea level rise (**Figure 11d**), the situation is rather different. Namely, uncertainties in the sea level rise due to thermal expansion of the deep ocean are primarily associated with the uncertainties in the climate parameters. This is explained by the large thermal inertia of the ocean, which significantly delays its response to changes in radiative forcing. Sokolov *et al*. (2007) carried out climate change simulations for three different combinations of climate parameters and two very different emissions scenarios. Their simulations showed that thermal sea level rise has practically no dependence on forcing through the year 2050. Even at the end of the 21st century sea level rise is more sensitive to changes in characteristics of the climate system than in emissions. Such behavior was also observed in simulations with the version of the IGSM2 in which a 3D ocean GCM was used instead of a 2D anomaly diffusing ocean model. Of course the impact of uncertainties in anthropogenic emissions on uncertainties in projected sea level rise will be much larger on longer time scales.

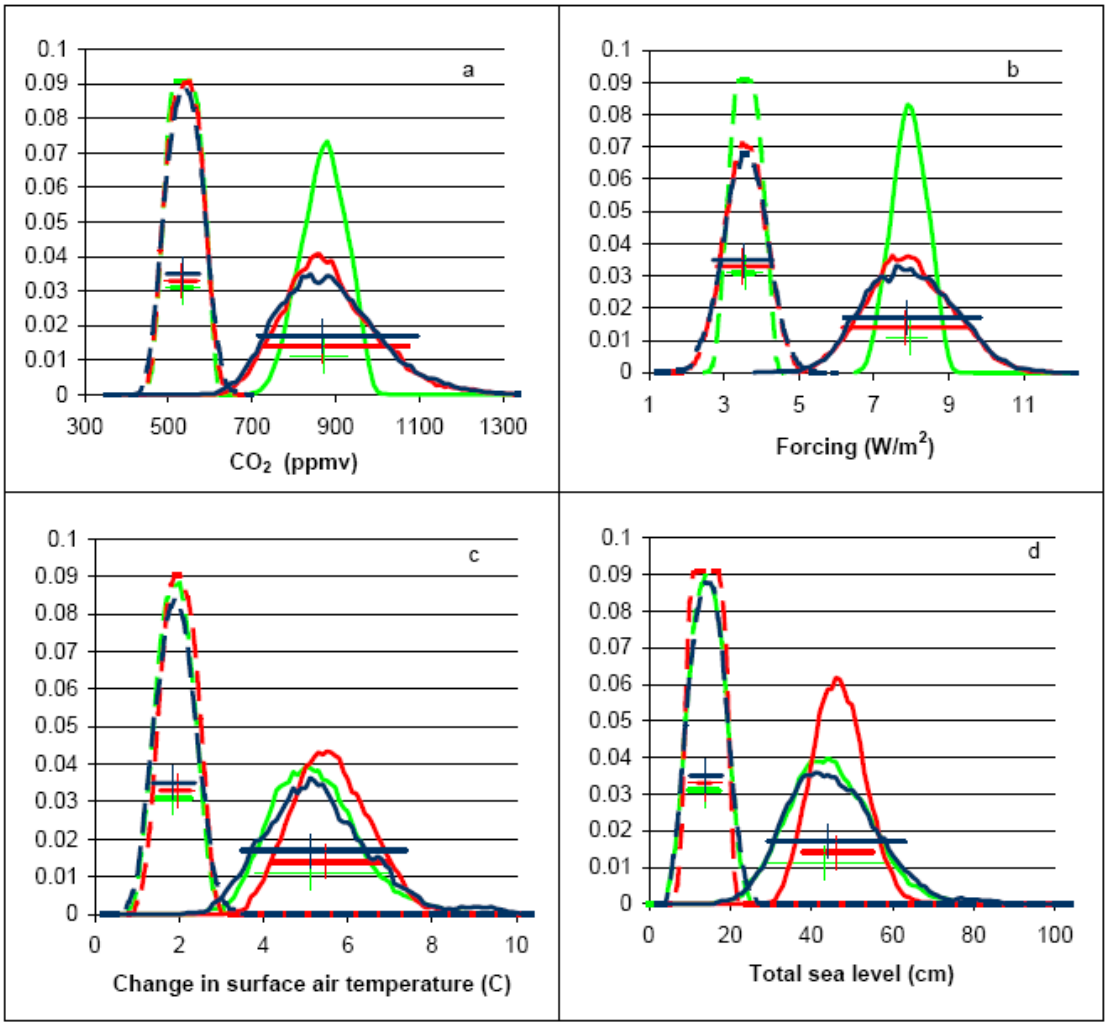

Figure 11. Frequency distributions for atmospheric CO_2 concentrations (a), radiative forcing due to GHGs and sulfate aerosol (b), surface air temperature (c), and total sea level rise (d). In simulations with full uncertainty (blue), climate uncertainty (green) and emissions uncertainty (red) averaged over 2041-2050 (dashed lines) and 2091-2100 (solid lines).

4.3 Changes in carbon fluxes

In addition to examining the statistical analysis of the model runs, it is instructive to examine a subset of runs in greater detail. Changes in global surface average temperature result from a combination of emissions and climate parameters, and therefore two runs that look similar in terms of temperature may be very different in detail. In this section four runs (**Table 3**) are examined in greater detail, especially in regards to fluxes of the major GHGs. A pair of scenarios was chosen from the 95% upper bound of surface temperature change (scenarios C and D), and the other pair was chosen from the 5% lower bound of surface temperature change (scenarios A and B). In each pair, one scenario had higher climate sensitivity but lower GHG concentrations than the other scenario with equivalent temperature (Table 3). High concentrations of different gases tend to be correlated with each other, as anthropogenic emissions of all these gases are driven by many of the same underlying factors such as economic growth rates (Webster *et al*. 2008).

Table 3. Values of climate parameters and values of some climate variables averaged over last decade of 21st century for the simulations discussed in section 5.3.

Scenario	CS	Kv	Faer	Kc	SAT	CO_2	CH_4	N_2O
A	1.83	0.22	-0.46	350	3.68	885	4.15	440.16
B	3.75	3.21	-0.65	384	3.70	622	3.30	413.38
C	2.55	0.10	-0.59	468	7.49	1108	5.44	450.83
D	4.10	0.96	-0.58	196	7.49	886	4.15	444.75

Concentrations of GHGs in the atmosphere are a function of sources and sinks. Anthropogenic emissions are the primary driver of changing GHG concentrations, but there are also natural sources of N_2O and CH_4, mainly in terrestrial wetlands. There are a number of sinks involved for the three major GHGs - ecosystems, oceans, atmospheric chemistry, and stratospheric disassociation. Most of the non-anthropogenic sinks and sources are functions of temperature, precipitation, and chemical or radiative interactions with other emissions, and these interactions are examined in more detail in this section.

As discussed by Sokolov *et al*. (2008a) the terrestrial ecosystem response to increased CO_2 concentrations is limited by nitrogen availability. However, surface warming leads to an increase in carbon uptake as the resulting increased soil matter decomposition releases nitrogen thereby allowing the ecosystem to take advantage of the higher CO_2 levels. However, when surface air temperature exceeds a critical value increase in respiration may overcome increase in gross primary productivity resulting in the decrease of net terrestrial carbon uptake. The critical value of SAT depends on changes in atmospheric CO_2 concentration and the value of the half-saturation constant (*kc*). For example, in case D terrestrial uptake peaks at 3 GtC/year near year 2080 and starts to decrease after increases in SAT exceeds 5.5°C (**Figure 12**). At the same time, in scenario C, despite similar surface warming, terrestrial carbon uptake increases through the whole simulation due to large values of *kc* used in this simulation and a larger increase in the atmospheric CO_2 concentration. In some of the hottest cases the terrestrial ecosystem becomes a net carbon source during the last decade of 21st Century. In all four cases, carbon uptake by the

terrestrial ecosystem is rather significant, on the order of 15 to 20% of anthropogenic emissions - cumulative uptake ranges from 215 GtC in scenario B to 350 GtC in scenario C.

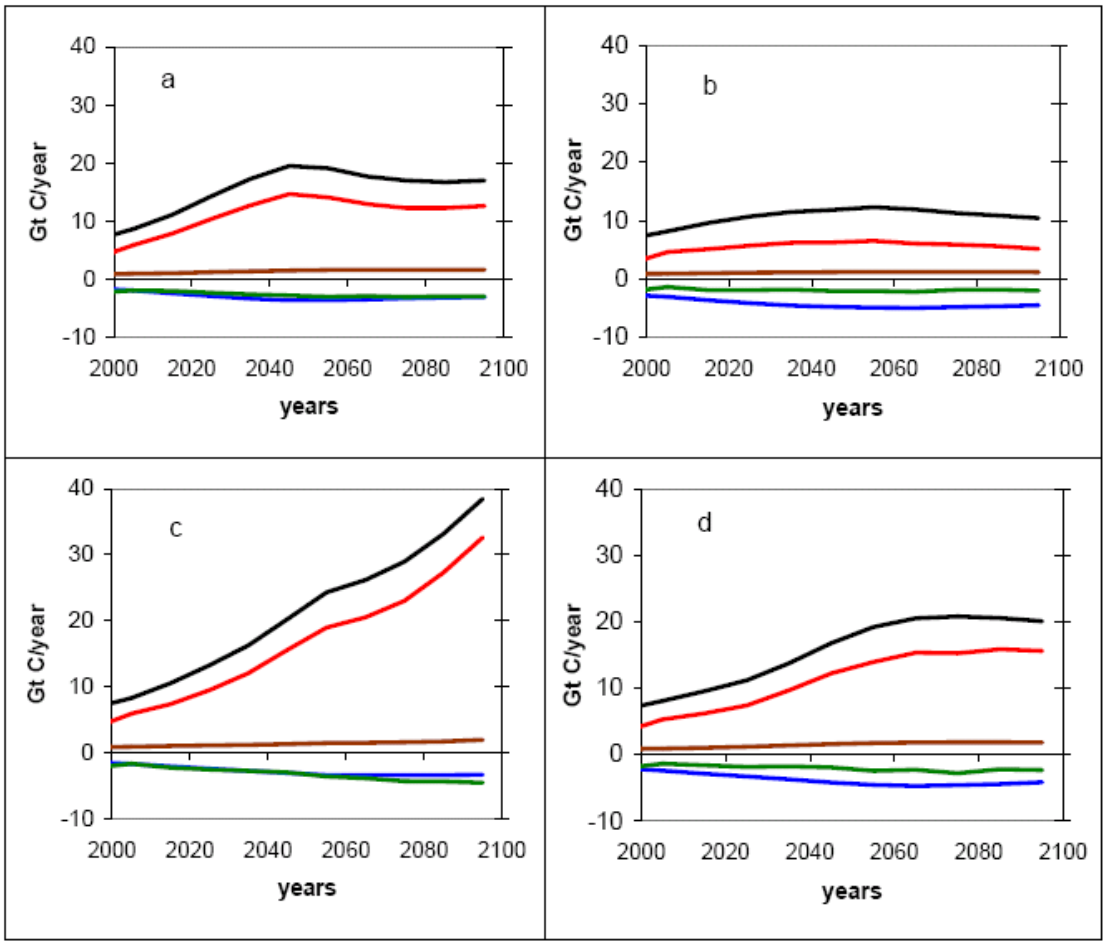

Figure 12. Carbon fluxes in gigatons of carbon/year. Black: anthropogenic CO_2 emissions. Green: terrestrial sink. Blue: ocean sink. Brown: CO and CH_4 emissions. Red: Change in atmospheric burden.

Ocean uptake is the other major CO_2 sink. Section 2.4 discusses how the carbon sink in IGSM2.2 is calibrated to reproduce the behavior of the 3-dimensional ocean. One of the important results of this calibration is that the end of century uptake is significantly lower than it would be in the version of the simplified carbon model used by Webster *et al*. (2003). In all four runs ocean uptake peaks midcentury and begins to decrease despite the continuing increases in atmospheric CO_2 concentration. However, the ocean still takes up a cumulative total of 300 GtC (scenario C) to 470 GtC (scenario B).

The Natural Ecosystems Model (NEM) controls the emissions of methane and N_2O into the atmosphere. As precipitation and temperature increase it is expected that natural emissions of both substances will also increase, but the exact nature of these increases depends on timing of precipitation events. High latitude regions (north of 50°N) exhibit a somewhat larger flux increase than the remainder of the globe, especially in the hot scenarios (C and D) where

northern latitude emissions (green dashed line in **Figure 13**) increase by more than 70% while the flux from the remainder of the planet increases by only 33% and 24%, respectively.

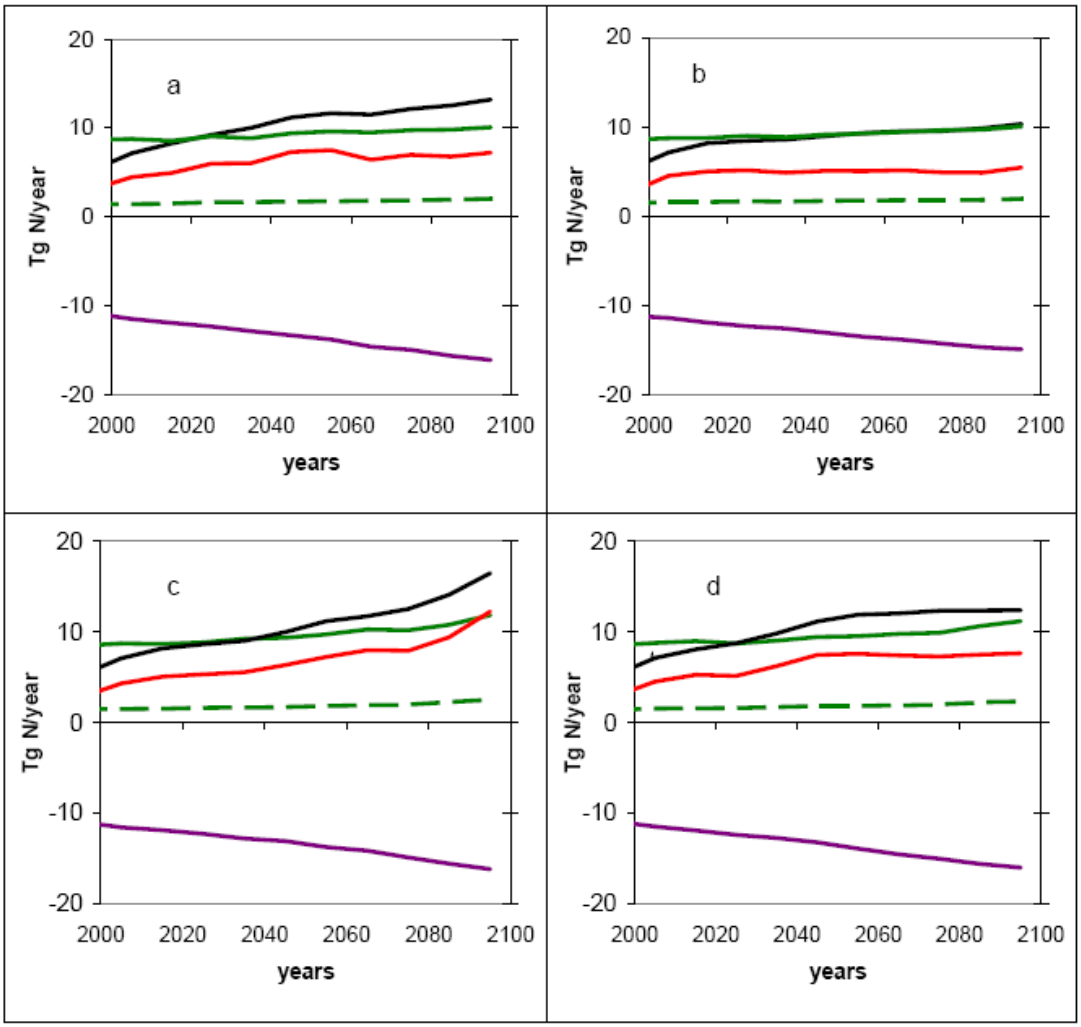

Figure 13. N_2O fluxes in Tg N/year. Black: anthropogenic emissions. Green: natural emissions. Dashed green: Northern latitude emissions. Purple: stratospheric sink. Red: Change in atmospheric burden.

Increased methane emissions are also expected to be prevalent in high latitude regions (north of 50°N) due to thawing of permafrost and increased CO_2 fertilization of plants (Zhuang *et al*. 2006). In the two warm runs high latitude emissions of methane increase by more than 150% (**Figure 14**: dotted green lines), compared to increases in the remainder of the planet of about 35%. Cumulatively, more than 3 gigatons of additional methane due to increased high latitude emissions are released into the atmosphere in both of the warm runs. This release of methane only accounts for a small fraction of the carbon stored in the soils of these high latitude regions, and emissions can be expected to continue to increase significantly after 2100.

Methane concentrations are also a function of the atmospheric sink, mainly the hydroxyl free radical. As CO and CH_4 emissions increase, the hydroxyl radical concentrations will drop as seen in section 4.1. When OH levels drop, the CH_4 sink will decrease and methane lifetime will

increase. This impact on CH_4 levels can be roughly estimated by plotting methane concentrations in the hypothetical case where lifetime does not decrease (Figure 14, dotted line). In both the hot scenarios (C and D) the cumulative sink decrease over the century is equivalent to about twelve gigatons of methane emissions.

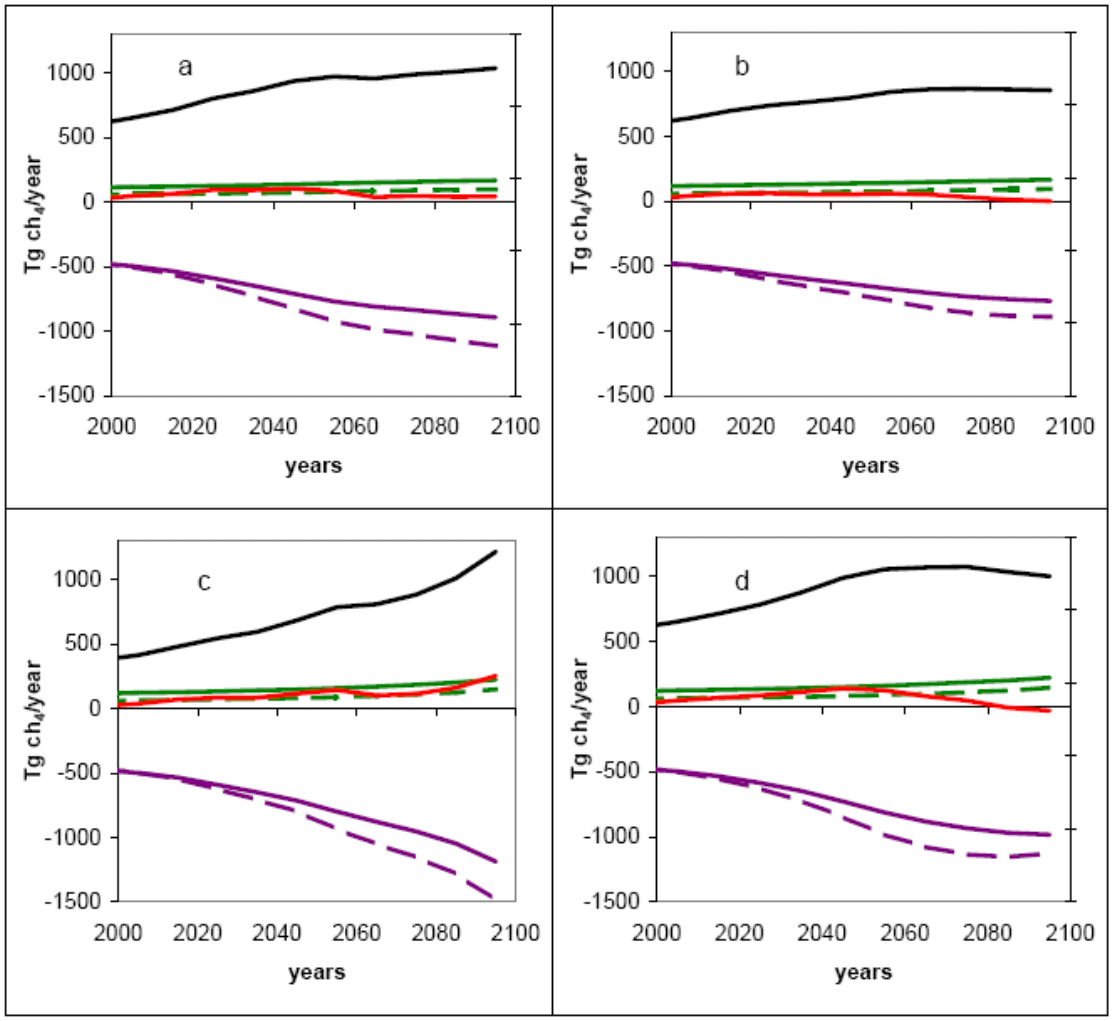

Figure 14. Methane fluxes in Tg CH_4/year. Black: anthropogenic emissions. Green: natural emissions. Dashed green: northern latitude emissions. Purple: methane sink. Dashed purple: Constant lifetime counterfactual sink.

4.4 Comparison with the IPCC AR4 projections

As discussed in the introduction, the treatment of uncertainty in anthropogenic emissions in this study is fundamentally different from that by the IPCC. The climate simulations described in the IPCC AR4 (Meehl *et al*. 2007a) were carried out for several distinctly different emission scenarios, either assuming 'business-as-usual' economic activities (A2, A1FI), or aimed at atmospheric CO_2 stabilization at a particular level (A1B and B2). However no probabilities were associated with these different emissions scenarios. Uncertainties in the climate response for a given emission scenario were associated only with uncertainty in the characteristics of the

climate system (Meehl *et al*. 2007a, Knutti *et al*. 2008). Therefore the IPCC AR4 results should be compared with the results of our ensemble of simulations in which only climate uncertainty was included while GHG emissions were calculated using median values of the uncertain economic parameters (see section 3.4).

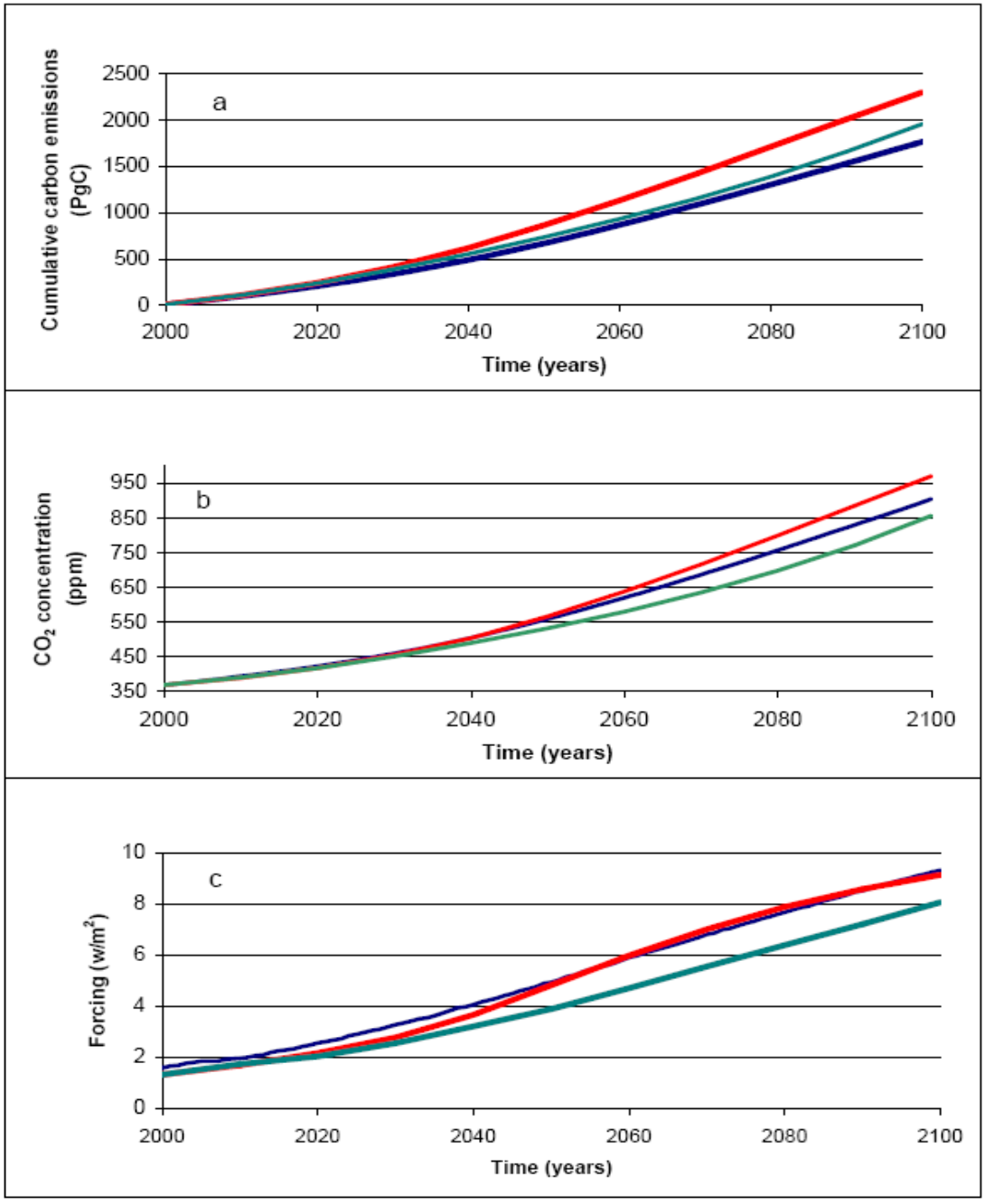

Figure 15. Cumulative carbon emissions (a), atmospheric CO_2 concentration (b) and radiative forcing due to greenhouse gases and aerosol (c) for SRES scenarios A1FI (red) and A2 (green) and for MIT simulation (blue) with median values for economic and climate input parameters.

The cumulative carbon emissions produced by the EPPA model with these parameter values are very similar to those for the A2 scenario and somewhat smaller than those in the A1FI scenario (see **Figure 15a**). However, the atmospheric CO_2 concentration obtained in the simulation with the IGSM using the median values of both the emission and climate parameters is closer to the concentration in the A1FI scenario (**Figure 15b**). This is explained, at least partly, by the fact that the terrestrial ecosystem model used in the IGSM2, in contrast to the ISAM model used to calculate CO_2 concentrations for the SRES scenarios, considers carbon/nitrogen interactions. As shown by Sokolov *et al* (2008a), taking into account the nitrogen limitation on terrestrial carbon uptake leads to a large increase in atmospheric CO_2 for given carbon emissions. The forcings due to individual GHGs (CH4, N2O, etc.) are somewhat different for our median emission scenario and for A1FI, but the total forcings are quite similar **(Figure 15c**). Thus it is appropriate to compare our results for the ensemble of simulations including only the climate model uncertainties with the IPCC's projections for the A1FI scenario. More detailed comparison between MIT and SRES scenarios is given by Prinn *et al*. (2008).

Since the AR4 AOGCMs did not simulate the A1FI scenario, the IPCC calculated the mean value of SAT increase for the A1FI scenario from 19 simulations with the Simple Climate Model (SCM MAGGIC, Wigley and Raper, 2001). The 19 different versions of the SCM were each tuned to simulate the behavior of a different one of the 19 AOGCMs used in the IPCC AR4 (Meehl *et al*. 2007a). The mean of the 19 SCM simulations was scaled to allow for a small bias in the SCM compared to the AOGCMs simulations for other scenarios (Meehl *et al*. 2007a, Knutti *et al*. 2008). Because, as noted by Meehl *et al*. (2007a), AOGCMs do not sample the full range of possible warming, the IPCC AR4's projected likely range (Solomon *et al*. 2007) of warming is not based solely on the 19 simulations but was estimated with the help of results of additional studies (Knutti *et al*. 2008), including simulations with models of intermediate complexity. Some of the models of intermediate complexity in addition to uncertainties in climate sensitivity, rate of oceanic heat uptake, strength of aerosol forcing and carbon cycle consider uncertainty in the feedback between the carbon cycle and climate (e.g. Knutti *et al*. 2003). Thus the *likely* range of warming was judged to extend from 40% less to 60% more than the mean SAT increase (Meehl *et al*. 2007a, Knutti *et al*. 2008). We note that, according to the IPCC AR4 definition, the probability of SAT change falling into the *likely* range is more than 66% but less than 90%.

Table 4. Change is SAT at the last decade of 21st century relative to 1981-2000, at year 2100 for Meinshausen et al (2008)

	5%	16.7%	Mean	83.3%	95%
MIT simulations with median anthropogenic emissions	3.81	4.22	5.17	6.04	6.98
Meinshausen et al (2008) (with uncertainty in feedback between climate and carbon cycle) for SRES A1FI	2.85	3.26	4.09	4.79	5.88
SCM MAGIC (with carbon uptake uncertainty) for SRES A1FI		3.30	4.40	5.80	
IPCC AR4 for SRES A1FI		2.40	4.00	6.40	

Table 4 compares the IPCC's mean and *likely* range of SAT increase for the A1FI scenario with those based on the results of the simulations with the latest version of the SCM MAGIC (Meinshausen *et al* 2008), tuned to 19 AR4 AOGCMs, and with those from our simulations with median anthropogenic emissions.

As discussed by Sokolov *et al* (2008b), the AR4 multi-model ensemble underestimate surface warming compared to MIT simulations with input parameters distributions obtained using Levitus *et al*. (2005) data on changes in deep ocean heat content. The same, of course, is true for the SCM MAGIC. In particular, our mean SAT increase is 30% greater than the IPCC's. The uncertainty range obtained in the MIT simulations is both narrower and more symmetric than the range given by the IPC. i.e., the lower bound of the 90% range is smaller than the mean by 26% while the upper bound is larger by 35% (**Table 5**). The asymmetry in the IPCC range is, to a large extent, associated with the uncertainty in the carbon cycle/climate feedback. As indicated by Knutti *et al*. (2008), inclusion of the uncertainty in carbon cycle/climate feedback as simulated by the C4MIP models (Friedlingstein *et al*. 2006) extends the projected range of surface warming, with larger effect on the upper bound. In contrast with all models used by the IPCC the MIT IGSM takes into account the carbon/nitrogen interaction in the terrestrial ecosystem. As was shown by Sokolov *et al*. (2008a), considering this interaction significantly reduces the strength of the feedback between the carbon cycle and climate and the uncertainty in the projected CO_2 concentration and surface warming associated with this feedback.

Table 5. Ratios of the percentiles values to the means for probability distributions shown in Table 4.

	5%	16.7%	83.3%	95%
MIT simulations with median anthropogenic emissions	0.74	0.82	1.17	1.35
Meinshausen et al (2008) (with uncertainty in feedback between climate and carbon cycle) for SRES A1FI	0.70	0.80	1.17	1.44
SCM MAGIC (with carbon uptake uncertainty) for SRES A1FI		0.77	1.35	
IPCC AR4 for SRES A1FI	0.60		1.60	

4.5 Sensitivity of the projected surface warming to the deep-ocean data used to derive climate input parameters

Sokolov *et al*. (2008b) compared results of ensembles of projections with the climate component of the MIT IGSM carried out using distributions of climate input parameters obtained with different data for changes in deep ocean heat content. As noted in the introduction, for the comparison with our previous results (Webster *et al*. 2003), we decided to use climate parameter distributions based on the Levitus *et al*. (2005) data in our simulations. We refer to these distributions as the LEV05 distributions. However, results presented by Sokolov *et al*. (2008b) allow us to approximate the distribution of changes in SAT for different climate parameter distributions without running a full ensemble of simulations. In this section we show how our results would have changed if we have had used input distributions for climate parameters based either on Domingous *et al*. (2008) or on upper and surface air temperatures only, DOM08 and

NO, respectively. We note that the LEV05 and DOM08 analyses give, respectively, the smallest and largest published estimates of the heat uptake (Sokolov *et al*. 2008b).

As can be seen from the Sokolov *et al*. (2008b), the shapes of the distributions for changes in SAT in the simulations with different distributions of climate input parameters are similar. In other words, ratios of the percentile values to the means do not differ significantly for ensembles with different input climate parameters (see Table 5 in Sokolov *et al*. (2008b)). This similarity between output distributions may be explained by the fact that projected surface warming is defined by joint input distributions, which are constrained by the same data on SAT changes over the 20th century. Based on that, the probability distribution for changes in SAT for a particular input distribution can be constructed by scaling the output distribution from the ensemble of simulations, carried out with different input distribution, by the ratio of the SAT changes in the simulations with the median values of input climate parameters from the two input distributions. **Table 6** shows the alternative distributions for cases with climate only uncertainty and full uncertainty.

Table 6. Distributions for changes in SAT at the last decade of 21st century for different choices of climate parameters distributions.

		5%	16.7%	Mean	83.3%	95%
Full uncertainties	LEV05	3.50	4.12	5.28	6.42	7.37
	NO	3.30	3.88	4.96	6.04	6.93
	DOM08	2.70	3.17	4.06	4.94	5.67
Climate only uncertainties	LEV05	3.81	4.22	5.17	6.04	6.98
	NO	3.58	3.97	4.87	5.68	6.57
	DOM08	2.93	3.25	3.98	4.65	5.38

For both uncertainty cases, the mean value of surface warming in the last decade of the 21st century decreases by about 0.3^{o}C for the NO and 1.2^{o}C for the DOM08 climate parameter distributions. Thus the DOM08 case has a mean warming very close to the IPCC's projection. .In the simulations with full (climate only) uncertainties, the probability for an SAT increase exceeding 6.4^{o}C by the end of the century decreases from 17% (12%) for LEV05 to 2.7% (0.5%) for DOM08 input climate distributions. The probability of surface warming being less than 2.4^{o}C is about 2.8% and 1.2% for the DOM08 distribution for the full and climate only uncertainty cases, respectively. For the LEV05 distributions SAT increases by more than 2.4^{o}C in all simulations for either uncertainty case. According to the IPCC AR4 projections the probability of SAT increase larger than 6.4^{o}C or smaller than 2.4^{o}C for theA1FI scenario is estimated as being between 5% and 16.7%. The much smaller likelihood we find for modest warming is likely due to our input pdfs having been explicitly constrained by 20th century temperature changes.

Projections of sea-level rise due to thermosteric expansion are much more sensitive to the ocean data used than are the projections of SAT (Sokolov *et al*. 2008b). However, probability distributions for sea level rise cannot be constructed using the scaling approach described above.

The comparisons just discussed do not per se tell us which of the three different projections compared in Table 6 is best. We note that the results based on LEV05 and DOM08 each used the

error estimates given by the respective analyses as being appropriate for their estimates of the trend in ocean warming. However these estimates are mutually incompatible. The DOM85 trend is more than double the LEV05 trend, but the difference between the two trends is five/seven times the standard deviation in the trend cited by the respective analyses. All this emphasizes an urgent necessity for obtaining more definite estimates for changes in deep-ocean heat content.

5. CONCLUSIONS

In this paper we have presented updated projections of climate changes for the 21st century in the absence of any climate policy. While the MIT IGSM has been significantly modified since publication of our previous projections (Webster *et al*. 2003), the primary reasons for the differences between our previous and present results are changes in the distributions of input parameters for both the earth system and economic components of the IGSM.

The simulations of 20th century climate used to estimate uncertainties in the climate system parameters (Forest *et al*. 2006 and 2008) were carried out using both anthropogenic and natural forcings. As discussed by Forest *et al.* (2006), taking into account natural forcings, especially forcing due to volcanic eruptions, led to significantly different distributions of climate system parameters compared to the distributions based on 20th century simulations with just anthropogenic forcings (Forest *et al*. 2002), which was used by Webster *et al*. (2003). The main consequence of the changes in the climate input distributions is an increase in the lower bound of the distribution of surface warming in response to an external forcing.

Similarly, the distributions of global GHGs emissions used in this study (Webster *et al*. 2008) are higher, compared with previous results (Webster *et al*. 2002) due to the reduction of very low emissions growth cases. One of the key differences is that GDP growth, while still more important than many other parameters, is not the primary driver of uncertainty in emissions. This change is a result of the new approach of generating GDP growth paths using a random walk, and of the assumption that GDP growth shocks are not correlated across countries. From this analysis, the primary drivers of uncertainty in no-policy carbon emissions are technological change, both price driven (e.g., elasticity of substitution) and non-price driven (e.g., autonomous energy efficiency improvement), and the total fossil resources available, particularly coal and shale (Webster *et al*. 2008). These changes in projected GHGs emissions noticeably decreased the probability of low radiative forcing.

Due to the multiplicative nature of the interaction between the forcing and the climate system response, the probability distribution of the increase in surface air temperature at the end of the 21st century is shifted upward significantly compared to the distribution obtained by Webster *et al*. (2003). As can be expected from the changes in the forcing and the response described above, the biggest difference is a sharp decrease in the probability of small or moderate warming. While the upper bound of the 90% range has increased by about 60%, the lower bound of the 90% range of the new distribution is more than 3 times larger than in the Webster *et al*. (2003).

While our median anthropogenic emissions are similar to those for the SRES A2 scenario, the GHGs concentrations simulated by the MIT IGSM are somewhat higher than those used in

the simulations with the IPCC AR4 AOGCMs. These differences in GHG concentrations arise from the different treatment of the terrestrial ecosystem and from the fact that we take into account an increase in the natural CH_4 and N_2O emissions caused by the surface warming, as well as from differences in chemistry models (Prinn *et al*. 2008). As a result, the total radiative forcing in our simulations with median anthropogenic emissions is quite close to the forcing for the IPCC A1FI scenario. However, the surface warming projected by the MIT IGSM significantly exceeds the estimates given by Meehl *et al*. (2007a). The shape of the probability distribution of changes in SAT simulated by the MIT IGSM is also different from that assumed by the IPCC AR4. The distribution obtained in our simulations is almost symmetric while the IPCC's distribution implies a long upper tail. Asymmetry in the IPCC distribution is, in part, explained by the larger impact of the uncertainty in the feedback between the climate and the carbon cycle on the upper bound of the surface warming range. Taking into consideration the interaction between carbon and nitrogen in the terrestrial ecosystem model reduces the strength of this feedback and the uncertainty in surface warming associated with it (Sokolov *et al*. 2008a).

All the ensembles of simulations presented in this paper were carried out with climate input parameter distributions based on the Levitus *et al*. (2005) estimate of changes in the deep ocean heat content. We also derived approximate distributions of changes in SAT for climate parameter distributions based on alternate estimates of the ocean heat uptake. These estimates suggest somewhat smaller surface warming. However, the probability of the SAT increase at the end of the 21st century being near 2^{o}C-2.5^{o}C is significantly lower than that suggested by the IPCC AR4 for all the distributions tested.

Acknowledgments

We would to thank Malte Meinshausen for providing results of the simulations with SCM MAGIC version 6 and Reto Knutii for useful discussion of SCM results. This work was supported in part by the Office of Science (BER), U.S. Department of Energy Grant No. DE-FG02-93ER61677, NSF, and by the MIT Joint Program on the Science and Policy of Global Change. We thank Josh Willis for discussions on the ocean heat content data. We acknowledge the modeling groups, the Program for Climate Model Diagnosis and Intercomparison (PCMDI) and the WCRP's Working Group on Coupled Modelling (WGCM) for their roles in making available the WCRP CMIP3 multi-model dataset. Support of this dataset is provided by the Office of Science, U.S. Department of Energy.

6. REFERENCES

Babiker, M.H., J.M. Reilly, M. Mayer, R.S. Eckaus, I. Sue Wing, and R.C. Hyman, 2001: The MIT Emissions Prediction and Policy Analysis (EPPA) Model: Revisions, Sensitivities, and Comparisons of Results. MIT Joint Program on the Science and Policy of Global Change, Report 71, 90 pp, (Available on line at: http://web.mit.edu/globalchange/www/MITJPSPGC_Rpt71.pdf)

Babiker, M.H., G.E. Metcalf, and J. Reilly 2003: Tax distortions and global climate policy, *Journal of Environmental Economics and Management*, **46**, 269-287.

Bonan, G.B., K.W. Oleson, M. Vertenstein, S. Lewis, X. Zeng, Y. Dai, R.E. Dickinson, and Z.-

L. Yang, 2002: The land surface climatology of the Community Land Model coupled to the NCAR Community Climate Model. *J. Climate*, **15**, 3123-3149.

Calbó, J., W. Pan, M. Webster, R.G. Prinn, and G.J. McRae, 1998: Parameterization of urban sub-grid scale processes in global atmospheric chemistry models. *J. Geophysical Research*, **103**, 3437-3451.

Curtis, P.S., and X. Wang, 1998: A meta-analysis of elevated CO_2 effects on woody plant mass, form, and physiology. *Oecologia*, **113,** 299-313.

Dalan, F., P.H. Stone, I. Kamenkovich, and J. Scott, 2005a: Sensitivity of the ocean's climate to diapycnal diffusivity in EMIC. Part I: Equilibrium state. *J. Climate*, **18**, 2460-2481.

Dalan, F., P.H. Stone, and A.P. Sokolov, 2005b: Sensitivity of the ocean's climate to diapycnal diffusivity in EMIC. Part II: Global warming scenario. *J. Climate*, **18**, 2482-2496.

Dimaranan, B., and R. McDougall, 2002: Global Trade, Assistance, and Production: The GTAP 5 Data Base. Center for Global Trade Analysis, Purdue University, West Lafayette, Indiana.

Domingues, C.M., J.A. Church, N.J. White, P.J. Gleckler, S.E. Wijffels, P.M. Barker, and J. R. Dunn, 2008: Improved estimates of upper-ocean warming and multi-decadal sea-level rise. *Nature*, **453**, 1090-1094.

Edmonds, J. A., and J.M. Reilly, 1985: Future global energy and carbon dioxide emissions. Chapter 9 in *Atmospheric Carbon Dioxide and the Global Carbon Cycle*, (J. Trabalka, ed.), US Department of Energy, Office of Energy Research, DOE/ER-0239, Washington DC: 215-246.

Felzer, B., J. Reilly, J. Melillo, D. Kicklighter, M. Sarofim, C. Wang, R. Prinn, and Q. Zhuang, 2005: Future effects of ozone on carbon sequestration and climate change policy using a global biogeochemical model. *Climatic Change*, **73**, 345-373.

Felzer, B., D.W. Kicklighter, J.M. Melillo, C. Wang, Q. Zhuang, and R. Prinn, 2004: Effects of ozone on net primary production and carbon sequestration in the conterminous United States using a biogeochemistry model. *Tellus* , **56B**, 230-248.

Follows, M.J., T. Ito, and S. Dutkiewicz, 2006: A Compact and Accurate Carbonate Chemistry Solver for Ocean Biogeochemistry Models. *Ocean Model,* **12**, 290-301.

Forest, C.E., P.H. Stone and A.P. Sokolov, 2008: Constraining Climate Model Parameters from Observed 20th Century Changes. *Tellus,* **60A**, 911-920.

Forest, C.E., P.H. Stone, and A.P. Sokolov, 2006: Estimated PDFs of Climate System Properties Including Natural and Anthropogenic Forcings. *Geophys. Res. Lett.,* **33**, L01705, http://dx.doi.org/doi:10.1029/2005GL023977.

Forest, C.E., P.H. Stone, A.P. Sokolov, M.R. Allen, and M. Webster, 2002: Quantifying uncertainties in climate system properties with the use of recent climate observations. *Science*, **295**, 113-117.

Friedlingstein, P., P. Cox, R. Betts, L. Bopp, W. von Bloh, V. Brovkin, P. Cadule, S. Doney, M. Eby, I. Fung, G. Bala, J. John, C. Jones, F. Joos, T. Kato, M. Kawamiya, W. Knorr, K. Lindsay, H.D. Matthews, T. Raddatz, P. Rayner, C. Reick, E. Roeckner, K.-G. Schnitzler, R. Schnur, K. Strassmann, A.J. Weaver, C. Yoshikawa, and N. Zeng, 2006: Climate–Carbon Cycle Feedback Analysis: Results from the C^4MIP Model Intercomparison. *J. Climate*, **19**, 3337-3353.

Gouretski, V., and K.P. Koltermann, 2007: How much is the ocean really warming? *Geophys. Res. Let.*, **34,** L01610, http://dx.doi.org/doi:10.1029/2006GL027834.

Gunderson, C.A., and S.D. Wullschleger, 1994: Photosynthetic acclimation in trees to rising

atmospheric CO_2: a broader perspective. *Photosynthesis Research,* **39**, 369-388.
Hansen, J., M. Sato, L. Nazarenko, R. Ruedy, A. Lacis, D. Koch, I. Tegen, T. Hall, D. Shindell, B. Santer, P. Stone, T. Novakov, L. Thomason, R. Wang, Y. Wang, D. Jacob, S. Hollandsworth, L. Bishop, J. Logan, A. Thompson, R. Stolarski, J. Lean, R. Willson, S. Levitus, J. Antonov, N. Rayner, D. Parker, and J. Christy, 2002: Climate forcings in Goddard Institute for Space Studies SI2000 simulations. *J. Geophys. Res.,* **107**, 4347.
Hansen, J., I. Fung, A. Lacis, D. Rind, S. Lebedeff, R. Ruedy, and G. Russell, 1988: Global climate change as forecast by goddard institute for space studies three-dimensional model, *J. Geophys. Res.* **93**, 9341-9364.
Hansen, J., A. Lacis, D. Rind, G. Russell, P. Stone, I. Fung, R. Ruedy, and J. Lerner, 1984: Climate Sensitivity: Analysis of Feedback Mechanisms. In*: Climate Processes and Climate Sensitivity, Geophysical Monograph* [Hansen, J.E., and T. Takahashi, (eds.)], **29**. American Geophysical Union, Washington, D.C.
Hansen, J., G. Russell, D. Rind, P. Stone, A. Lacis, S. Lebedeff, R. Ruedy, and L. Travis, 1983: Efficient three-dimensional global models for climate studies: Models I and II. *Monthly Weather Review*, **111**, 609-662.
Hegerl, G.C., F.W. Zwiers, P. Braconnot, N.P. Gillett, Y. Luo, Marengo J.A. Orsini, N. Nicholls, J.E. Penner, P.A. Stott, 2007: Understanding and Attributing Climate Change. In: *Climate Change 2007: The Physical Science Basis. Contribution of Working Group I to the Fourth Assessment Report of the Intergovernmental Panel on Climate Change* [Solomon, S., D. Qin, M. Manning, Z. Chen, M. Marquis, K.B. Averyt, M. Tignor, and H.L. Miller (eds.)]. Cambridge University Press, Cambridge, UK and New York, NY, USA.
Holian, G.L., A.P. Sokolov, and R.G. Prinn, 2001: Uncertainty in Atmospheric CO_2 Predictions from a Global Ocean Carbon Cycle Model. Report 80, MIT Joint Program on the Science and Policy of Global Change Report 80, 25 pp. (available on line at: http://web.mit.edu/globalchange/www/MITJPSPGC_Rpt80.pdf)
Houghton, J.T., Y. Ding, D.K. Griggs, M. Noguer, P.J., van der Linden, X. Dai, K. Maskell, and C.A. Johnson, (eds). 2001. *Climate Change 2001: The Scientific Basis. Contribution of Working Group I to the Third Assessment Report of the Intergovernmental Panel on Climate Change*. Cambridge University Press, Cambridge, United Kingdom and New York, NY, USA.
Iman, R.L., and J.C. Helton, 1988: An Investigation of Uncertainty and Sensitivity Analysis Techniques for Computer Models. *Risk Analysis* **8**, 71-90.
Jacoby, H., R. Eckaus, A.D. Ellermann, R. Prinn, D. Reiner, and Z. Yang, 1997: CO_2 Emissions Limits: Economic Adjustments and the Distribution of Burdens. *The Energy Journal,* **18**, 31-58.
Kamenkovich, I.V., A. Sokolov, and P.H. Stone, 2002: An efficient climate model with a 3D ocean and statistical-dynamical atmosphere. *Climate Dynamics,* **19**, 585-598.
Knutti, R., M.R. Allen, P. Friedlingstein, J.M. Gregory, G.C. Hegerl, G.A. Meehl, M. Meinshausen, J.M. Murphy, G.-K. Plattner, S.C.B. Raper, T.F. Stocker, P.A. Stott, H. Teng, and T.M.L Wigley. 2008: A review of uncertainties in global temperature projections over the twenty-first century. *J. Climate*, **21**, 2651–2663.
Knutti, R., T.F. Stoker, F. Joos, and G.-K. Plattner, 2003: Probabilistic climate change projections using neural network. *Climate Dynamics,* **21**, *257-272.*
Lean, J., 2000: Evolution of the sun's spectral irradiance since the Maunder Minimum. *Geophys. Res. Lett.*, **27**: 2421-2424.

Levitus, S., J. Antonov, and T.P. Boyer, 2005: Warming of the World Ocean, 1955–2003. *Geophys. Res. Lett.*, **32**, L02604, http://dx.doi.org/doi:10.1029/2004GL021592.

Li, C., S. Frolking, and T.A. Frolking, 1992: A model of nitrous oxide evolution from soil driven by rainfall events: 1. Model structure and sensitivity. *J. Geophys. Res.*, **97**, 9759-9776.

Liu, Y., 1996: Modeling the Emissions of Nitrous Oxide (N_2O) and Methane (CH_4) from the Terrestrial Biosphere to the Atmosphere. Ph.D. Thesis. MIT Joint Program on the Science and Policy of Global Change, Report 10, 219 pp. (Available on line at http://web.mit.edu/globalchange/www/MITJPSPGC_Rpt10.pdf)

Mayer, M., C. Wang, M. Webster, and R.G. Prinn, 2000: Linking local air pollution to global chemistry and climate. *J. Geophys. Res.*, **105**, 22869-22896.

McGuire, A.D., J.M. Melillo, D.W. Kicklighter, Y. Pan, X. Xiao, J. Helfrich, B. Moore III, C.J. Vorosmarty, and A.L. Schloss, 1997: Equilibrium responses of global net primary production and carbon storage to doubled atmospheric carbon dioxide: Sensitivity to changes in vegetation nitrogen concentration. *Global Biogeochem. Cycles,* **11,** 173-189.

McGuire, A.D., L.A. Joyce, D.W. Kicklighter, J.M. Melillo, G. Esser, and C.J. Vorosmarty, 1993: Productivity response of climax temperate forests to elevated temperature and carbon dioxide: a North American comparison between two global models. *Climatic Change* **24,** 287-310.

McGuire, A.D., J.M. Melillo, L.A. Joyce, D.W. Kicklighter, A.L. Grace, B. Moore III, and C. J. Vorosmarty, 1992: Interactions between carbon and nitrogen dynamics in estimating net primary productivity for potential vegetation in North America. *Global Biogeochem. Cycles* **6,** 101-124.

Meehl, G.A., T.F. Stocker, W.D. Collins, P. Friedlingstein, A.T. Gaye, J.M. Gregory, A. Kitoh, R. Knutti, J.M. Murphy, A. Noda, S.C.B. Raper, I.G. Watterson, A.J. Weaver, and Z.-C. Zhao, 2007a: Global Climate Projections. In: *Climate Change 2007: The Physical Science Basis. Contribution of Working Group I to the Fourth Assessment Report of the Intergovernmental Panel on Climate Change* [Solomon, S., D. Qin, M. Manning, Z. Chen, M. Marquis, K.B. Averyt, M. Tignor and H.L. Miller (eds.)]. Cambridge University Press, Cambridge, United Kingdom and New York, NY, USA.

Meehl, G. A., C.Covey, T. Delworth, M. Latif, B. McAvaney, J. F.B. Mitchell, R.J. Stouffer, and K. E.Taylor, 2007b: The WCRP CMIP3 Multimodel Dataset: A New Era in Climate Change Research. *Bull. American Meteorological Society*, **88**, 1383–1394.

Meinshausen, M., S.C.B. Raper, and T.M.L. Wigley, 2008: Emulating IPCC AR4 atmosphere-ocean and carbon cycle models for projecting global-mean, hemispheric and land/ocean temperatures: MAGICC 6.0. *Atmospheric Chemistry and Physics Discussions,* **8**, 6153-6272, http://www.atmos-chem-phys-discuss.net/8/6153/2008/acpd-8-6153-2008.html.

Melillo, J.M., A.D. McGuire, D.W. Kicklighter, B. Moore III, C.J. Vorosmarty, and A.L. Schloss, 1993: Global climate change and terrestrial net primary production. *Nature*, **363**, 234-240.

Moss, R.H., and S.H. Schneider, 2000: Towards Consistent Assessment and Reporting of Uncertainties in the IPCC TAR. In: *Cross-Cutting Issues in the IPCC Third Assessment Report* [Pachauri, R., and T. Taniguchi (eds.)]. Cambridge University Press, Cambridge, UK.

Morgan, M.G., and D. Keith, 1995: Subjective Judgments by Climate Experts. *Environmental Science & Technology*, **29**, 468-476.

Nakicenovic, N., *et al*., 2000: *Special Report on Emissions Scenarios, Intergovernmental Panel on Climate Change.* Cambridge University Press, Cambridge, UK.

Norby, R.J., E.H. DeLucia, B. Gielen, C. Calfapietra, C.P. Giardina, J.S. King, J. Ledford, H.R. McCarthy, D.J.P. Moore, R. Ceulemans, P. De Angelis, A.C. Finzi, D.F. Karnosky, M.E. Kubiske, M. Lukac, K.S. Pregitzer, G.E. Scarascia-Mugnozza, W.H. Schlesinger, and R. Oren, 2005: Forest response to elevated CO_2 is conserved across a broad range of productivity. *PNAS*, **102**, 18052-18056.

Norby, R.J., S.D. Wullschleger, C.A. Gunderson, D.W. Johnson, and R. Ceulemans, 1999: Tree responses to rising CO_2: implications for the future forest. *Plant, Cell and Environment* **22,** 683-714.

Nordhaus, W.D., and G.W. Yohe, 1983: Future paths of energy and carbon dioxide emissions, In: *Changing Climate, Report of the Carbon Dioxide Assessment Committee of the National Academy of Science*, National Academy Press, Washington DC: 87-152.

Olivier, J.G.J., and J.J.M. Berdowski, 2001: Global emission sources and sinks. In: *The Climate System* [Berdowski, J., R. Guicherit and B.J. Heij (eds.)]. Lisse: Swets & Zeitlinger Publishers. EDGAR 3.2 by RIVM/TNO, pp. 33-77.

Paltsev, S., J.M. Reilly, H.D. Jacoby, R.S. Eckaus, J. McFarland, M. Sarofim, M. Asadoorian, and M. Babiker (2005): The MIT Emissions Prediction and Policy Analysis (EPPA) Model: Version 4, MIT Joint Program for the Science and Policy of Global Change, Report 125, 72 pp. (Available on line at http://web.mit.edu/globalchange/www/MITJPSPGC_Rpt125.pdf)

Paltsev, S., J. Reilly, H. Jacoby, A. Gurgel, G. Metcalf, A. Sokolov, and J. Holak, 2008: Assessment of US GHG Cap-and-Trade Proposals, *Climate Policy* (in press).

Pan, Y., J.M. Melillo, A.D. McGuire, D.W. Kicklighter, L.F. Pitelka, K. Hibbard, L.L. Pierce, S.W. Running, D.S. Ojima, W.J. Parton, D. S.Schimel, and other VEMAP Members, 1998: Modeled responses of terrestrial ecosystems to elevated atmospheric CO_2: A comparison of simulations by the biogeochemistry models of the Vegetation/Ecosystem Modeling and Analysis Project (VEMAP). *Oecologia,* **114,** 389-404.

Peixoto, J.P. and A.H. Oort, 1992: Phisics of Climate, AIP, New York, 520 pp.

Plattner, G.-K., R. Knutti, F. Joos, T.F. Stocker, W. von Bloh, V. Brovkin, D. Cameron, E. Driesschaert, S. Dutkiewicz, M. Eby, N. R. Edwards, T. Fichefet, C. D. Jones, M.F. Loutre, H.D. Matthews, A. Mouchet, S.A. Müller, S. Nawrath, A. Price, A. Sokolov, K.M. Strassmann, and A.J. Weaver, 2008; Long-term climate commitments projected with climate-carbon cycle models. *J. Climate*, **21**, 2721- 2751.

Prinn, R., S. Paltsev, A. Sokolov, M. Sarofim, J. Reilly, and H. Jacoby, 2008: The Influence on Climate Change of Differing Scenarios for Future Development Analyzed Using the MIT Integrated Global System Model, MIT Joint Program for the Science and Policy of Global Change, Rep. 163. 28 pp. (Available on line at http://globalchange.mit.edu/files/document/MITJPSPGC_Rpt163.pdf)

Prinn, R., J. Reilly, M. Sarofim, C. Wang, and B. Felzer, 2007: Effects of air pollution control on climate: results from an integrated assessment model. in: *Human-induced Climate Change: An Interdisciplinary Assessment* [M.E. Schlesinger, H.S. Kheshgi, J. Smith, F.C. de la Chesnaye, J.M. Reilly, T. Wilson, and C. Kolstad (eds.)]. Cambridge University Press, Cambridge, UK.

Prinn, R., H. Jacoby, A. Sokolov, C. Wang, X. Xiao, Z. Yang, R. Eckaus, P. Stone, D. Ellerman, J. Melillo, J. Fitzmaurice, D. Kicklighter, G. Holian, and Y. Liu, 1999: Integrated global system model for climate policy assessment: Feedbacks and sensitivity studies. *Climatic Change*, **41**, 469-546.

Raich, J.W., E.B. Rastetter, J.M. Melillo, D.W. Kicklighter, P.A. Steudler, B.J. Peterson, A.L. Grace, B. Moore III, and C.J. Vorosmarty, 1991: Potential net primary productivity in South America: application of a global model. *Ecological Applications* **1,** 399-429.

Reilly, J., J. Edmonds, R. Gardner, and A. Brenkert, 1987: Monte Carlo Analysis of the IEA/ORAU Energy/Carbon Emissions Model, *The Energy Journal*, **8**, 1-29.

Reilly, J., and S. Paltsev, 2006: European Greenhouse Gas Emissions Trading: A System in Transition. In: *Economic Modeling of Climate Change and Energy Policies* [De Miguel, M. *et al* (eds.)]. Edward Elgar Publishing, 45-64.

Reilly, J., R. Prinn, J. Harnisch, J. Fitzmaurice, H. Jacoby, D. Kicklighter, J. Mellilo, P. Stone, A. Sokolov, and C. Wang, 1999: Multi-gas assessment of the Kyoto Protocol. *Nature*, **401**, 549-555.

Russell, G.L., J.R. Miller, and L-C Tsang, 1985: Seasonal ocean heat transport computed from an atmospheric model. *Dyn. Atmos. Oceans,* **9**, 253-271.

Rutherford, T. (1995): *Demand Theory and General Equilibrium: An Intermediate Level Introduction to MPSGE*, GAMS Development Corporation, Washington, DC.

Sato, M., J.E. Hansen, M.P. McCormick, and J.B. Pollack, 1993: Stratospheric aerosol optical depths. *J. Geophys. Res.*, **98**, 22987-22994.

Schlosser, C.A., D. Kicklighter, and A. Sokolov, 2007: A global land system framework for integrated climate-change assessments. MIT Joint Program for the Science and Policy of Global Change, Report 147, 82 pp. (Available on line at http://web.mit.edu/globalchange/www/MITJPSPGC_Rpt147.pdf)

Schlosser, C.A., and Webster, M.D., 2008:. A Probabilistic Description of Precipitation Frequency Change in Climate Models. (forthcoming).

Smith, S.J, R. Andres, E. Conception, and J. Lurz, 2004. Historical Sulfur Dioxide Emissions 1850-2000: Methods and Results. PNNL Research Report 14537, Pacific Northwest National Laboratory.

Sokolov, A.P., D.W. Kicklighter, J.M. Melillo, B. Felzer, C.A. Schlosser, and T.W. Cronin, 2008a: Consequences of Considering Carbon/Nitrogen Interactions on the Feedbacks Between Climate and the Terrestrial Carbon Cycle, *J. Climate*, **21**, 3776-3796.

Sokolov, A.P., C.E. Forest, and P.H. Stone, 2008b: Sensitivity of climate change projections to uncertainties in the estimates of observed changes in deep-ocean heat content. *Climate Dynamics*, submitted. (Also available as MIT Joint Program for the Science and Policy of Global Change Report 166, 14 pp. http://web.mit.edu/globalchange/www/MITJPSPGC_Rpt166.pdf)

Sokolov, A.P., S. Dutkiewicz, P.H. Stone, and J.R. Scott, 2007: Evaluating the use of ocean models of different complexity in climate change studies. MIT Joint Program for the Science and Policy of Global Change Report 128, 23 pp. (Available on line at http://web.mit.edu/globalchange/www/MITJPSPGC_Rpt128.pdf)

Sokolov, A.P. 2006: Does model sensitivity to changes in CO2 provide a measure of sensitivity to other forcings? *J. Climate*, **19**, 3204–3306.

Sokolov, A.P., C.A. Schlosser, S. Dutkiewicz, S. Paltsev, D.W. Kicklighter, H.D. Jacoby, R.G. Prinn, C.E. Forest, J. Reilly, C. Wang, B. Felzer, M.C. Sarofim, J. Scott, P.H. Stone, J.M. Melillo, and J. Cohen, 2005: The MIT Integrated Global System Model (IGSM) Version 2: Model Description and Baseline Evaluation, MIT Joint Program for the Science and Policy of Global Change Report 124, 40 pp. (Available on line at http://web.mit.edu/globalchange/www/MITJPSPGC_Rpt124.pdf)

Sokolov, A., and P.H. Stone, 1998: A flexible climate model for use in integrated assessments. *Climate Dynamics*, **14**: 291-303.
Sokolov, A.P., C. Wang, G. Holian, P.H. Stone, and R. Prinn, 1998: Uncertainty in the Oceanic Heat and Carbon Uptake and their Impact on Climate Projections, *Geophys. Res. Lett.,* **25**, 3603-3606.
Solomon, S., D. Qin, M. Manning, Z. Chen, M. Marquis, K.B. Averyt, M. Tignor, and H.L. Miller (eds.), 2007: *Climate Change 2007: The Physical Science Basis*. Cambridge University Press, Cambridge UK.
Stern, D.I., 2006: Reversal of the trend in global anthropogenic sulfur emissions. *Global Environmental Change* **16**, 207-220.
Stern, D.I., 2005: Beyond the Environmental Kuznets Curve: Diffusion of Sulfur-Emissions-Abating Technology. *Journal of Environment and Development* **14**, 101-124.
Stocker, T.F., W.S. Broecker and D.G. Wright, 1994: Carbon Uptake Experiments with a Zonally-Averaged Global Ocean Circulation Model. *Tellus* **46B**, 103-122.
Stone, P.H., and M.-S. Yao, 1990: Development of a two-dimensional zonally averaged statistical-dynamical model. III: The parameterization of the eddy fluxes of heat and moisture. *J. Climate*, **3**: 726-740.
Stone, P.H., and M.-S. Yao, 1987: Development of a two-dimensional zonally averaged statistical-dynamical model. II: The role of eddy momentum fluxes in the general circulation and their parameterization. *J. Atmospheric Science*, **44**, 3769-3536.
Tatang, M.A., W. Pan, R.G. Prinn, and G.J. McRae, 1997: An efficient method for parametric uncertainty analysis of numerical geophysical models. *J. Geophys. Res.*, **102**: 21925-21932.
US CCSP [United States Climate Change Science Program] (2007): *CCSP Synthesis and Assessment Product 2.1, Part A: Scenarios of Greenhouse Gas Emissions and Atmospheric Concentrations*, L. Clarke *et al*. US Climate Change Science Program, Department of Energy, Washington, DC.
Wang, C., 2004: A modeling study on the climate impacts of black carbon aerosols. *J. Geophys. Res.*, **109** (D03106), doi:10.1029/2003JD004084.
Wang, C., R.G. Prinn, and A. Sokolov, 1998: A global interactive chemistry and climate model: Formulation and testing. *J. Geophys. Res.*, **103**, 3399-3418.
Wang, Y., and D. Jacob, 1998: Anthropogenic forcing on tropospheric ozone and OH since preindustrial times. *J. Geophys. Res.*, **103**, 31,123-31,135.
Webster, M.D., S. Paltsev, J. Parsons, J. Reilly, and H. Jacoby,2008:. Uncertainty in greenhouse emissions and costs of atmospheric stabilization, MIT Joint Program for the Science and Policy of Global Change Report 165. (Available on line at http://web.mit.edu/globalchange/www/MITJPSPGC_Rpt165.pdf)
Webster, M., C. Forest, J. Reilly, M. Babiker, D. Kicklighter, M. Mayer, R. Prinn, M. Sarofim, A. Sokolov, P. Stone, and C. Wang, 2003: Uncertainty analysis of climate change and policy response. *Climatic Change*, **62**, 295-320.
Webster, M.D., M. Babiker, M. Mayer, J.M. Reilly, J. Harnisch, R. Hyman, M.C. Sarofim, and C. Wang, 2002: Uncertainty in emissions projections for climate models. *Atmospheric Environment*, **36**: 3659-3670.
Webster, M.D., and A.P. Sokolov, 2000: A Methodology for Quantifying Uncertainty in Climate Projections. *Climatic Change*, **46**, 417–446.
Wigley, T.M.L., and S.C.B. Raper, 2001: Interpretation of high projections for global-mean warming. *Science*, **293**, 451-454.

Wijffels, S.E.,J. Willis, C.M. Domingues, P. Barker, N.J White, A. Gronell, K. Ridgway, and J.A. Church, 2008: Changing eXpendable Bathythermograph Fallrates and their Impact on Estimates of Thermosteric Sea Level Rise. *J. Climate*, **21**, 5657–5672.

Yao, M-S, and Stone PH, 1987: Development of a two-dimensional zonally averaged statistical-dynamical model. Part I The parameterization of moist convection and its role in the general circulation. *J Atmos Sci,* **44**, 65-82.

Zhuang, Q., J.M. Melillo, M.C. Sarofim, D.W. Kicklighter, A.D. McGuire, B.S. Felzer, A. Sokolov, R.G. Prinn, P.A. Steudler, and S. Hu, 2006: CO_2 and CH_4 exchanges between land ecosystems and the atmosphere in northern high latitudes over the 21st century. *Geophys. Res. Lett.,* **33**, L17403, http://dx.doi.org/doi:10.1029/2006GL026972.

REPORT SERIES of the **MIT** *Joint Program on the Science and Policy of Global Change*

1. **Uncertainty in Climate Change Policy Analysis** *Jacoby & Prinn* December 1994
2. **Description and Validation of the MIT Version of the GISS 2D Model** *Sokolov & Stone* June 1995
3. **Responses of Primary Production and Carbon Storage to Changes in Climate and Atmospheric CO_2 Concentration** *Xiao et al.* October 1995
4. **Application of the Probabilistic Collocation Method for an Uncertainty Analysis** *Webster et al.* January 1996
5. **World Energy Consumption and CO_2 Emissions: 1950-2050** *Schmalensee et al.* April 1996
6. **The MIT Emission Prediction and Policy Analysis (EPPA) Model** *Yang et al.* May 1996 (*superseded by No. 125*)
7. **Integrated Global System Model for Climate Policy Analysis** *Prinn et al.* June 1996 (*superseded by No. 124*)
8. **Relative Roles of Changes in CO_2 and Climate to Equilibrium Responses of Net Primary Production and Carbon Storage** *Xiao et al.* June 1996
9. **CO_2 Emissions Limits:** ***Economic Adjustments and the Distribution of Burdens*** *Jacoby et al.* July 1997
10. **Modeling the Emissions of N_2O and CH_4 from the Terrestrial Biosphere to the Atmosphere** *Liu* Aug. 1996
11. **Global Warming Projections:** ***Sensitivity to Deep Ocean Mixing*** *Sokolov & Stone* September 1996
12. **Net Primary Production of Ecosystems in China and its Equilibrium Responses to Climate Changes** *Xiao et al.* November 1996
13. **Greenhouse Policy Architectures and Institutions** *Schmalensee* November 1996
14. **What Does Stabilizing Greenhouse Gas Concentrations Mean?** *Jacoby et al.* November 1996
15. **Economic Assessment of CO_2 Capture and Disposal** *Eckaus et al.* December 1996
16. **What Drives Deforestation in the Brazilian Amazon?** *Pfaff* December 1996
17. **A Flexible Climate Model For Use In Integrated Assessments** *Sokolov & Stone* March 1997
18. **Transient Climate Change and Potential Croplands of the World in the 21st Century** *Xiao et al.* May 1997
19. **Joint Implementation:** ***Lessons from Title IV's Voluntary Compliance Programs*** *Atkeson* June 1997
20. **Parameterization of Urban Subgrid Scale Processes in Global Atm. Chemistry Models** *Calbo* et al. July 1997
21. **Needed: A Realistic Strategy for Global Warming** *Jacoby, Prinn & Schmalensee* August 1997
22. **Same Science, Differing Policies;** ***The Saga of Global Climate Change*** *Skolnikoff* August 1997
23. **Uncertainty in the Oceanic Heat and Carbon Uptake and their Impact on Climate Projections** *Sokolov et al.* September 1997
24. **A Global Interactive Chemistry and Climate Model** *Wang, Prinn & Sokolov* September 1997
25. **Interactions Among Emissions, Atmospheric Chemistry & Climate Change** *Wang & Prinn* Sept. 1997
26. **Necessary Conditions for Stabilization Agreements** *Yang & Jacoby* October 1997
27. **Annex I Differentiation Proposals:** ***Implications for Welfare, Equity and Policy*** *Reiner & Jacoby* Oct. 1997
28. **Transient Climate Change and Net Ecosystem Production of the Terrestrial Biosphere** *Xiao et al.* November 1997
29. **Analysis of CO_2 Emissions from Fossil Fuel in Korea: 1961–1994** *Choi* November 1997
30. **Uncertainty in Future Carbon Emissions:** ***A Preliminary Exploration*** *Webster* November 1997
31. **Beyond Emissions Paths:** ***Rethinking the Climate Impacts of Emissions Protocols*** *Webster & Reiner* November 1997
32. **Kyoto's Unfinished Business** *Jacoby et al.* June 1998
33. **Economic Development and the Structure of the Demand for Commercial Energy** *Judson et al.* April 1998
34. **Combined Effects of Anthropogenic Emissions and Resultant Climatic Changes on Atmospheric OH** *Wang & Prinn* April 1998
35. **Impact of Emissions, Chemistry, and Climate on Atmospheric Carbon Monoxide** *Wang & Prinn* April 1998
36. **Integrated Global System Model for Climate Policy Assessment:** ***Feedbacks and Sensitivity Studies*** *Prinn et al.* June 1998
37. **Quantifying the Uncertainty in Climate Predictions** *Webster & Sokolov* July 1998
38. **Sequential Climate Decisions Under Uncertainty:** ***An Integrated Framework*** *Valverde et al.* September 1998
39. **Uncertainty in Atmospheric CO_2 (Ocean Carbon Cycle Model Analysis)** *Holian* Oct. 1998 (*superseded by No. 80*)
40. **Analysis of Post-Kyoto CO_2 Emissions Trading Using Marginal Abatement Curves** *Ellerman & Decaux* Oct. 1998
41. **The Effects on Developing Countries of the Kyoto Protocol and CO_2 Emissions Trading** *Ellerman et al.* November 1998
42. **Obstacles to Global CO_2 Trading:** ***A Familiar Problem*** *Ellerman* November 1998
43. **The Uses and Misuses of Technology Development as a Component of Climate Policy** *Jacoby* November 1998
44. **Primary Aluminum Production:** ***Climate Policy, Emissions and Costs*** *Harnisch et al.* December 1998
45. **Multi-Gas Assessment of the Kyoto Protocol** *Reilly et al.* January 1999
46. **From Science to Policy:** ***The Science-Related Politics of Climate Change Policy in the U.S.*** *Skolnikoff* January 1999
47. **Constraining Uncertainties in Climate Models Using Climate Change Detection Techniques** *Forest et al.* April 1999
48. **Adjusting to Policy Expectations in Climate Change Modeling** *Shackley et al.* May 1999
49. **Toward a Useful Architecture for Climate Change Negotiations** *Jacoby et al.* May 1999
50. **A Study of the Effects of Natural Fertility, Weather and Productive Inputs in Chinese Agriculture** *Eckaus & Tso* July 1999
51. **Japanese Nuclear Power and the Kyoto Agreement** *Babiker, Reilly & Ellerman* August 1999
52. **Interactive Chemistry and Climate Models in Global Change Studies** *Wang & Prinn* September 1999
53. **Developing Country Effects of Kyoto-Type Emissions Restrictions** *Babiker & Jacoby* October 1999

Contact the Joint Program Office to request a copy. The Report Series is distributed at no charge.

Contact the Joint Program Office to request a copy. The Report Series is distributed at no charge.

Contact the Joint Program Office to request a copy. The Report Series is distributed at no charge.